

Award Accounts

The Chemical Society of Japan Award for Young Chemists for 2007

Surface-Mediated Design and Catalytic Properties of Active Metal Complexes for Advanced Catalysis Creation

Mizuki Tada

Institute for Molecular Science, 38 Nishigo-naka, Myodaiji, Okazaki 444-8585

Received December 15, 2009; E-mail: mtada@ims.ac.jp

Molecular-scale design of catalytically active structures at oxide surfaces is highlighted, focusing on our recent challenges for selective heterogeneous catalysis. We found novel structural transformations of supported metal complexes on oxide surfaces and achieved unique selective catalysis for various chemical syntheses. In this account, the advanced design of supported metal-complex catalysts on oxide surfaces and the in situ characterization of their structural kinetics, which means kinetics of structural changes of catalysts themselves, under catalyst-working conditions are reviewed.

1. Surface-Mediated Design of Catalytically Active Structures for Selective Catalysis

1.1 Introduction: Metal-Complex Attaching on Oxide Surfaces. Heterogeneous solid catalysts have been widely utilized for the industrial production of many synthetic chemicals. The advantages of heterogeneous catalysts are not only the separation of catalysts and products from reaction media but also their high durability and catalytic activities resulting from the unique structures of catalytically active sites at solid surfaces. Relationships among the metal structures, organized environment, and the catalytic properties of surface species tell us the nature of catalysis and new strategy for rational design of heterogeneous catalysts.

Metal-complex attachment to oxide surfaces is a practical way to produce molecularly regulated structures of active metal species on oxide surfaces, and subsequent structural transformation in a controllable manner often provides unique regulated metal structures active for selective catalytic reactions.[1–16] There are several types of metal-complex attachment techniques: coordination of metal-complex precursors to immobilized ligands on organic polymers,[17–21] coordination of metal-complex precursors to functional ligands bound to oxide surfaces,[2,4,22–25] intercalation into clay materials,[26] ion exchange into porous materials such as zeolite and mesoporous silica,[27] and direct attachment of metal-complex precursor onto oxide surfaces.[3,6,11,28,29]

The interfacial attachment between a metal complex and an oxide surface can produce unique metal coordination different from the original metal-complex precursor. For example, Si–OH is reacted with a $M(CH_3)$ complex and a M(OSi) complex is produced, releasing CH_4. A chemical bond between a metal-complex precursor and a support surface modifies the reactivity of the supported metal complex, resulting in novel catalytic activity the precursor complex does not exhibit.[3,6,11,28,29] Traditional ion-exchange on zeolites and intercalation to clay materials are also typical ways to introduce metal species onto solid supports although the valences and types of metal precursors are restricted.[4] Direct reactions of metal-complex precursors and hydroxy groups on oxide surfaces create novel metal-coordination structures, and many important factors for selective catalysis can be controlled at the interface, such as electronic properties and coordination sphere of the attached metal center, geometry around the active metal center, and dispersion and stability of the attached metal sites.[11,28–31] In particular, the formation of unsaturated metal species, which cannot be isolated in homogeneous solution or self-assembled materials, is a key issue to enhance catalytic activity.

We have designed and prepared various supported metal-complex catalysts on oxide surfaces and found novel surface phenomena to achieve great performance for selective catalysis. Figure 1 shows our recent examples of the preparation of novel supported metal-complex catalysts on oxide surfaces.[11,28,29] In this chapter, the surface-mediated design of catalytically active metal complexes for selective catalysis is highlighted.

1.2 Reaction-Induced and Photoinduced Selective Formation of Active Ru Complexes on SiO_2 Surfaces. In homogeneous metal-complex catalyzed reactions, it is suggested that one of the ligands coordinated to a metal-complex catalyst is released to form a catalytically active unsaturated metal complex at an initial stage of a catalytic reaction. The low stability of such unsaturated active metal complex easily forms metal aggregates in solution, leading to a loss of catalytic activity. Metal-complex attachment on support surfaces enables such unsaturated active metal complexes to remain on oxide surfaces.[23,25,32,33]

Published on the web July 24, 2010; doi:10.1246/bcsj.20090336

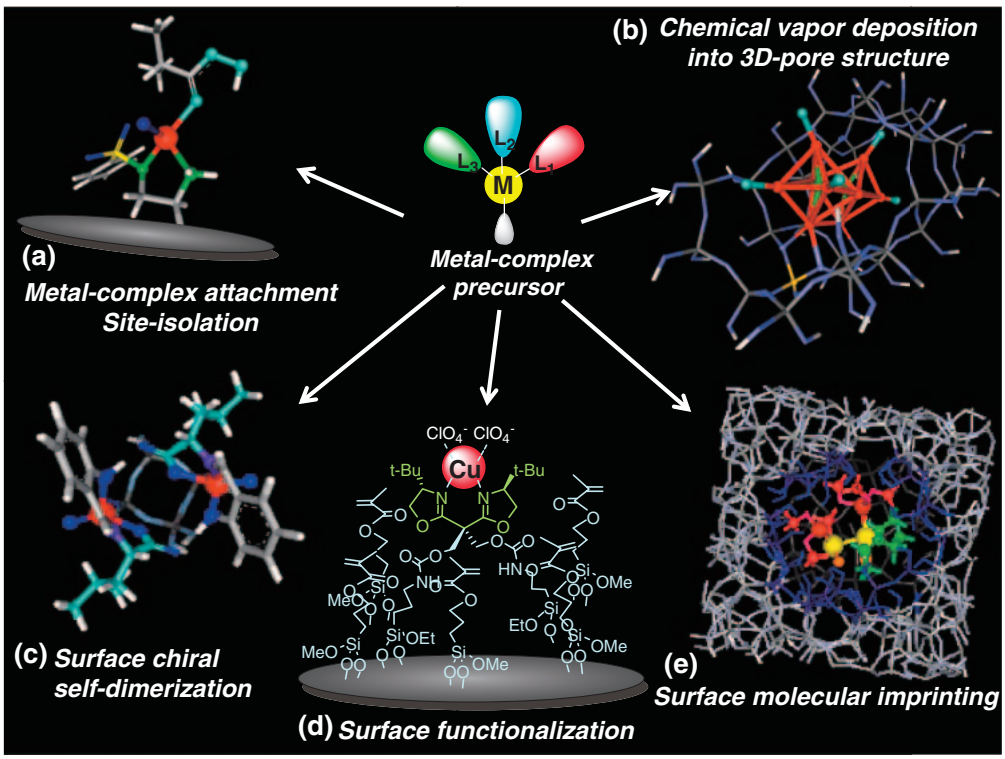

Figure 1. Advanced design of supported metal-complex catalysts on oxide surfaces.

A novel 3-coordinated unsaturated Ru complex can be prepared on the surface of SiO_2 by the exothermic reaction induced selective elimination of a *p*-cymene ligand in an immobilized Ru–*p*-cymene complex. A Ru precursor complex, a monomeric *p*-cymene-coordinated Ru–*N*-sulfonyl-1,2-ethylenediamine complex (**A**),[34] was tethered on SiO_2. The Ru complex (**A**) and its analogs are reported to be efficient for various catalytic reactions such as hydrogenation, oxidation, and isomerization.[35–39] It was found that an exothermic O_2/IBA (IBA: isobutyraldehyde) reaction induced the stoichiometric elimination of the *p*-cymene ligand, accompanied by the formation of an unsaturated Ru complex at the surface (**C**), which was highly active for alkene epoxidation.[23]

The immobilized Ru complex (**B**) was prepared in three steps, the procedure of which is illustrated in Figure 2. SiO_2 was functionalized with *p*-styryltrimethoxysilane, and the Ru precursor complex (**A**) was tethered onto the *p*-styryl-functionalized SiO_2 surface, forming a SiO_2-immobilized Ru complex (**B**) with a *p*-cymene ligand. ^{29}Si solid-state NMR revealed that the *p*-styryltrimethoxysilane reacted with Si–OH to be tethered on the SiO_2 surface by making the interfacial bonds $-Si(OSi)_3$ at −62 ppm (30%) and $-Si(-OSi)_2(-OCH_3)$ at 54 ppm (70%). UV–vis spectra and Ru K-edge EXAFS indicated that the local coordination of the Ru precursor complex (**A**) remained after attachment at the SiO_2 surface (Figure 2 (**B**)).

It was found that molecular oxygen and IBA stoichiometrically drove the *p*-cymene ligand out of the immobilized Ru center to selectively create a coordinatively unsaturated Ru complex at the SiO_2 surface, which was stable in air and recyclable for catalytic alkene epoxidation. Under O_2 atmosphere, 89% of *p*-cymene to Ru was released by the reaction of IBA and O_2, while no release of *p*-cymene was observed under N_2 atmosphere. The formed Ru complex (**C**) after the release of the *p*-cymene ligand, which was unsaturated, was found to be highly active for selective oxidation reactions.[23,40]

Hybrid DFT calculations suggested that the exclusive release of *p*-cymene from **B** without IBA was endothermic ($-66\,kJ\,mol^{-1}$), while the elimination of *p*-cymene using the reaction energy of IBA and O_2 was exothermic ($398\,kJ\,mol^{-1}$) as shown in Figure 2. Ru K-edge EXAFS curve-fitting analysis indicated the formed Ru complex (**C**) had an unsaturated Ru structure with two Ru–N bonds (coordination number (CN) = 2.2) at a distance of 0.207 nm and a Ru–Cl bond (CN = 1.3) at a distance of 0.234 nm. The coordination of O_2 (negatively charged as O_2^-) was suggested to stabilize the unsaturated Ru complex on the surface.[23] The reaction energy of IBA oxidation to isobutyric acid promoted the endothermic release of the *p*-cymene ligand from the supported Ru complex, resulting in the exothermic formation of the unsaturated active Ru complex. The unsaturated active Ru complex on SiO_2 was produced in conjunction with the exothermic IBA reaction in the coordination sphere.[23]

The supported Ru complex (**C**) was highly active for *trans*-stilbene epoxidation using IBA and O_2. The Ru precursor complex (**A**) in a homogeneous phase produced a small amount of *trans*-stilbene oxide (5 equivalents to Ru after 72 h and 71% of *trans*-stilbene oxide selectivity), but the reaction shortly stopped, forming black precipitates. On the other hand, the SiO_2-supported Ru complex (**C**) exhibited good catalytic performance under similar O_2/IBA reaction conditions: the TON of *trans*-stilbene was 50 (4 h) and *trans*-stilbene oxide selectivity was 83%. The epoxidation of other alkenes such as cyclopentene, norbornene, 1-octene, and styrene also smoothly proceeded on the supported Ru catalyst (**C**). The addition of

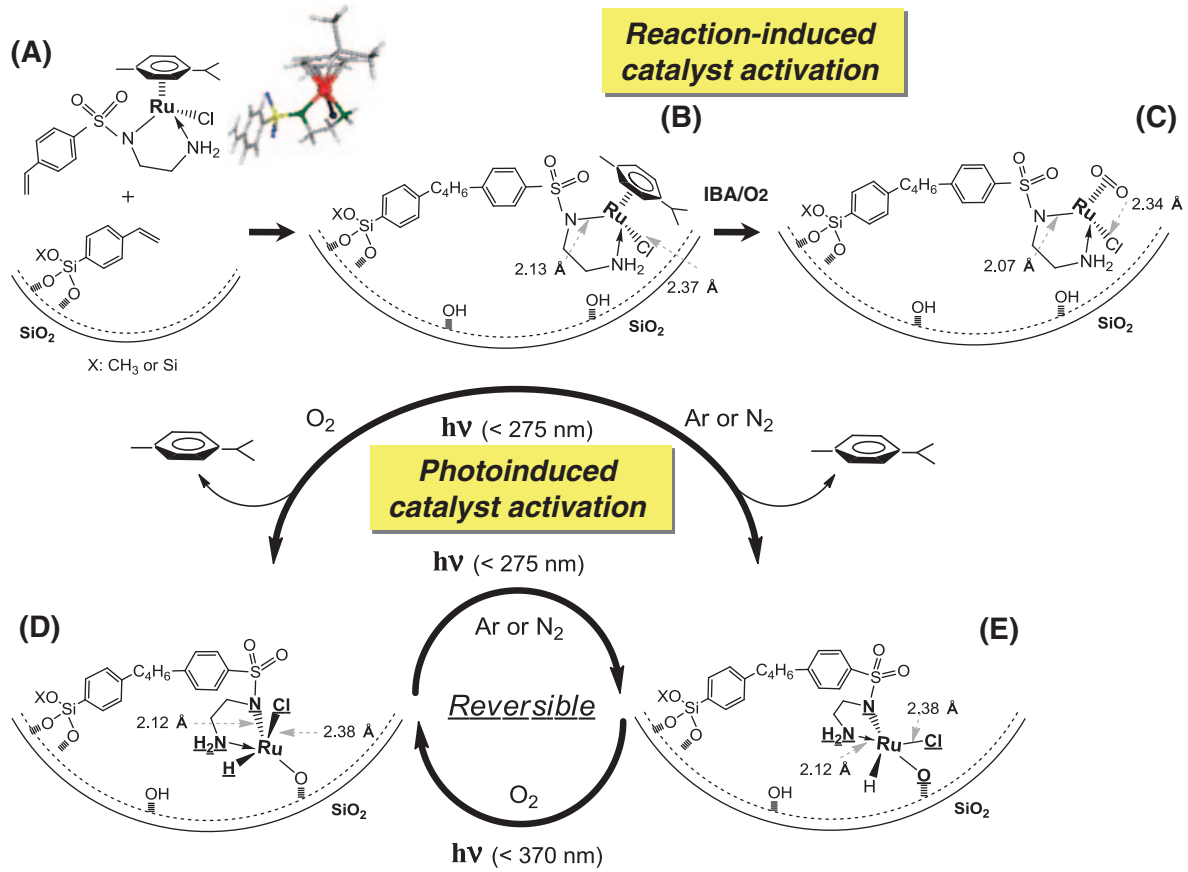

Figure 2. Reaction-induced and photoinduced selective formation of active Ru complexes supported on SiO_2.

SiO_2 into the homogeneous phase of **A** did not improve the deactivation so that the chemical grafting on the SiO_2 surface was key to prevent the active Ru complex from aggregating in reaction solution. The site-isolation of the Ru complex (**A**) on the SiO_2 surface provided high stability of the active Ru species and the TON of 2100000 was achieved on the supported Ru complex (**C**) for *trans*-stilbene epoxidation.[40]

We have found another catalyst activation method for the supported Ru complex (**B**), photoinduced selective formation of an active Ru complex on a SiO_2 surface.[41] The photoirradiation of the supported Ru complex (**B**) promoted the selective formation of two different Ru structures on the SiO_2 surface, depending on the atmosphere (O_2 or N_2), one of whose structures with an appropriate Ru–H conformation catalyzed selective photooxidation of cycloalkanes with O_2. The transformation between the two Ru structures was found to be reversible by photoexcitation with different wavelengths and atmospheres.

UV-light ($\lambda_{threshold} = 275$ nm) irradiation of **B** under N_2 brought about the stoichiometric elimination of the coordinated *p*-cymene ligand. The shift of XPS Ru $3d_{5/2}$ binding energy from 282.0 (**B**) to 282.2 eV (**E**) indicated that the surface Ru complex (**E**) was positively charged by the photoirradiation.[42–44] Ru K-edge EXAFS revealed two types of metal coordination, Ru–O(N) and Ru–Cl, whose CN were 3.2 at 0.210 nm and 1.0 at 0.238 nm, respectively, which indicated surface coordination to Ru forming Ru–O bonds in addition to the original immobilization using the *p*-styryl moiety. ^{13}C solid-state NMR indicated that the diamine ligand still remained during the photoinduced *p*-cymene elimination under N_2 (Figure 2 (**B**) → (**E**)).

Photoirradiation ($\lambda_{threshold} = 275$ nm) of **B** under O_2 also released *p*-cymene but produced a different structure (**D**). UV–vis spectra of **D** and **E** were different: **E** produced under N_2 had two peaks at 468 and 696 nm, while **D** produced under O_2 had a peak around 517 nm. It is to be noted that the transformation between these two structures (**D** and **E**) was reversible: **D** converted to **E** by photoirradiation ($\lambda_{threshold} = 370$ nm) under O_2 and **E** converted to **D** by photoirradiation ($\lambda_{threshold} = 275$ nm) under N_2. Surface Si–OH groups positively contributed to the photodissociation of the *p*-cymene ligand, and the cleavage of Si–OH provided two structural configurations (**D** and **E**) illustrated in Figure 2.[41]

The formed Ru complex (**D**) prepared under O_2 was found to be active for the selective photooxidation of cycloalkanes to the corresponding alcohols and ketones using O_2. Cyclohexane oxidation smoothly proceeded without an induction period for at least 6 h, and TON of the photooxidation reached 35 at 6 h with 96% selectivity. The thermal oxidation of cyclohexane did not proceed at 353 K.

It is to be noted that **E** prepared under N_2 was inactive for the photooxidation of cyclohexane. Iodometry suggested that Ru–OOH was an active species for the selective oxidation, and Ru–OOH may be formed by the insertion of O_2 to Ru–H on **D**. A vacant site on **E** was opposite the Ru–H bond and was geometrically inactive for Ru–OOH formation. **D**, of which Ru–H was adjacent to a vacant site smoothly produced active

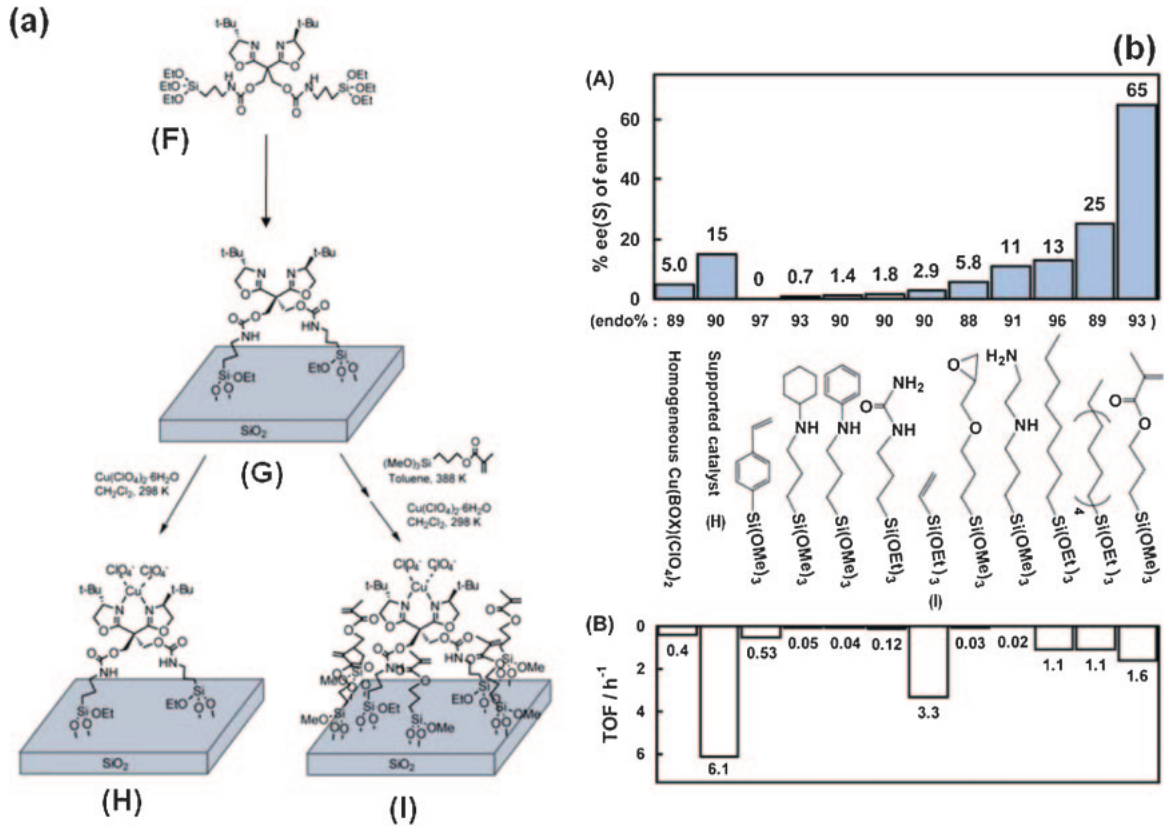

Figure 3. (a) Preparation steps of SiO_2-supported Cu–box catalysts by metal-complex attachment and surface functionalization with achiral organic molecules. (b) Their catalytic performances for Diels–Alder reactions of cyclopentadiene and 3-acryloyl-2-oxazolidinone at 263 K.

Ru–OOH on the SiO_2 surface. Photoinduced selective elimination of a *p*-cymene ligand in **B** brought about the dissociative coordination of a surface OH group to the unsaturated Ru center and the immobilization at double sites on the SiO_2 surface is suggested to be a key issue to produce the active species for the selective photooxidation using O_2.[41] These results show that the chemical bond with surfaces is a key factor to draw out catalytic activity and appropriate surfaces can produce new catalysis.

1.3 Chiral Amplification on SiO_2-Supported Cu–box Complex by Surface Functionalization with Achiral Molecules. Precise design of asymmetric metal-complex catalysts has been achieved for various asymmetric catalytic reactions in homogeneous phases.[45–48] Bis(oxazoline) (box) is a practical ligand for asymmetric catalysis, and it is well known that Cu–box complexes are useful for asymmetric Diels–Alder reactions,[49–57] which are widely used in pharmaceutics and biosynthesis.[58,59] Immobilized Cu–box catalysts have been also reported on nafion-silica,[60] amorphous silica,[61] microporous materials,[62] MCM-41,[63–65] and organic polymers.[66,67] We found that the functionalization of a Cu–box-supported SiO_2 surface with achiral organic molecules amplified the enantioselectivity of asymmetric Diels–Alder reaction between cyclopentadiene and 3-acryloyl-2-oxazolidinone on the supported Cu–box catalyst.[22,68]

SiO_2-supported and surface-functionalized Cu–box catalysts were prepared in a controllable manner as shown in Figure 3a. A box ligand with silane-coupling moieties (**F**) was grafted on SiO_2, and a SiO_2-supported box ligand (**G**) was obtained. The surface of box ligand grafted SiO_2 was functionalized with silane-coupling reagents such as (a) *p*-styryltrimethoxysilane, (b) 3-cyclohexylaminopropyltrimethoxysilane, (c) 3-phenylaminopropyltrimethoxysilane, (d) ureidopropyltriethoxysilane, (e) triethoxyvinylsilane, (f) 3-glycidoxypropyltrimethoxysilane, (g) 3-(2-aminoethylamino)propyltrimethoxysilane, (h) octyltriethoxysilane, (i) octadecyltriethoxysilane, and (j) 3-methacryloxypropyltrimethoxysilane, and then $Cu(ClO_4)_2 \cdot 6H_2O$ was coordinated to the box ligands on both surfaces with and without the functionalizing reagents (Figure 3a (**H**) and (**I**)). The amount of the supported box ligand was estimated to be 0.03 mmol g^{-1} (0.1 box molecule nm^{-2}) by δ_{C-H} peak intensity at 1370 cm^{-1} in FT-IR.

ESR signal of the supported Cu–box complex (**H**) was observed at higher magnetic fields than that of a $Cu(ClO_4)_2$ precursor, which indicated that the precursor was coordinated to the immobilized box ligand.[69] A peak observed around 370 nm for the supported Cu–box catalyst (**H**) in diffuse-reflectance UV–vis spectra suggested the similar local coordination to a homogeneous analog $[Cu(box)(ClO_4)_2]$. The bond distance and total CN of Cu–O and Cu–N in the supported Cu–box catalyst (**H**) were 0.199 ± 0.001 nm and 4.4 ± 0.5, respectively by Cu K-edge EXAFS. Similar structural parameters were also observed for the surface-functionalized Cu–box catalysts (**I**), indicating that the local coordination of the both Cu–box complexes on the SiO_2 surface (**H**) and (**I**) were similar to $[Cu(box)(ClO_4)_2]$ as shown in Figure 3a.[22]

Catalytic Diels–Alder reaction of cyclopentadiene and 3-acryloyl-2-oxazolidinone smoothly proceeded on the supported Cu–box complex without surface functionalization (**H**) as shown in Figure 3b. It is to be noted that the surface functionalization using achiral molecules enhanced the enantioselectivity of the Diels–Alder reaction (Figure 3b). In particular, in the case of (j) 3-methacryloxypropyltrimethoxysilane, the surface-functionalized Cu–box catalyst (**I**) brought about a large increase in the enantioselectivity. It was found that further surface-functionalization up to a full coverage of (j), 0.6 mmol g^{-1}, increased the enantioselectivity to 65% ee of endo product. The addition of free (j) to the simple immobilized Cu–box catalyst (**H**) did not enhance the enantioselectivity. Thus, the chemical bonding of (j) to the surface was indispensable and the full-coverage functionalization with (j) was most effective for the promotion of enantioselective catalysis.

Other silane-coupling reagents with styryl (a) and vinyl (e) groups caused large decreases in the enantioselectivity (Figure 3b). Long alkyl chains such as octyl (h) and octadecyl (i) groups influenced ee to a degree. Enantioselectivity for the longer octadecyl group (i) (25% ee) was higher than 13% ee for the shorter octyl group (h), while their catalytic activities were similar. Cyclohexylamino (b), phenylamino (c), urea (d), epoxy (f), and amino (g) compounds brought about large loss of the catalytic activities because these reagents act as bidentate ligands for Cu^{2+} probably decomposing the original Cu–box coordination.

Only the methacryl-functionalized catalyst (**I**-j) exhibited high enantioselectivity for the Diels–Alder reaction. As the lengths of the methacryl reagent (j) and the box ligand on SiO_2 were similar to each other, the oxygen of the methacryl group may interact with the NH group of the chiral box ligand by hydrogen bonding. The dependency of the enantioselectivity on the coverage of (j) indicated that the achiral methacryl groups surrounded the supported chiral box ligand to form a new assembled structure of the chiral box with the achiral methacryl groups, resulting in the large increase in ee on the surface. The enantiomeric excess in polar $CHCl_3$ and ethanol were as small as 0.8 and 5% ee, respectively, also agreeing with the assumption of the assembled structure on the surface. This gluing effect of achiral methacryl groups on the chiral box ligand may be the origin of the increase in the chiral selectivity.[22,68]

1.4 Surface Chiral Self-Dimerization of V Schiff-Base Complexes for Asymmetric Oxidative Coupling. Heterogeneous asymmetric catalysis is still a serious challenge to be tackled and the immobilization of chiral metal complexes has been reported to prepare heterogeneous asymmetric catalysts.[22,60,61,70,71] We found a novel chiral self-dimerization of V Schiff-base complexes on SiO_2[72,73] to produce novel asymmetric reaction space on a surface two V-monomer complexes were spontaneously dimerized via a selective reaction with surface Si–OH groups and resultant hydrogen bonding. The chiral self-dimerized V complexes exhibited high enantioselectivity for the asymmetric oxidative coupling of 2-naphthol to 1,1′-binaphthol (BINOL), whose derivatives have been utilized as versatile chiral sources for asymmetric catalysis.[74–94]

The attachment of V-monomer complexes (**J**) with several chiral Schiff-base ligands was performed by impregnation. The Ph–O moiety of the Schiff-base ligand reacted with surface Si–OH leading to the structural reconstruction of V-coordination as shown in Figure 4 (**K**). The Ph–O moiety selectively transformed to Ph–OH, and the V Schiff-base complex was grafted via a V–O–Si bond to the SiO_2 surface. The formed Ph–OH moiety showed hydrogen bonding with a C=O moiety of another V complex and a chiral reaction space was created between two unsaturated V centers. The formation of the chiral reaction space between two activated metal centers automatically proceeded on the SiO_2 surface, called surface chiral self-dimerization.

The curve-fitting analysis of V K-edge EXAFS Fourier transforms revealed the supported V complex (**K**) had an unsaturated conformation, which was different from that of the V-monomer precursor (**J**). There were two kinds of chemical bonding of a V=O bond at 0.157 ± 0.001 nm and V–O bonds at 0.199 ± 0.002 nm, and coordination number (CN) of the V–O bonds decreased from 3.8 ± 0.4 to 2.8 ± 0.5 after the attachment on the SiO_2 surface. The decrease in the CN of V–O by the support was observed in the V loading range of 0.3–3.4 wt %. Longer-distance bonding was not observed for all the SiO_2-supported catalysts, indicating that there was no direct V–V bonding in the supported V catalysts (**K**).[72,73]

All coordination sites of the Schiff-base ligand to the V^{4+} center possessed infrared active functional groups, Ph–O, Ph ring, C=N, and COO: three frequencies (1598, 1373, and 1362 cm^{-1}) were assigned as one $\nu_{asym(COO)}$ and two $\nu_{sym(COO)}$; 1629 cm^{-1} peak was assigned to $\nu_{(C=N)}$; four peaks of 1547, 1470, 1447, and 1436 cm^{-1} were referred to $\nu_{(Ph)}$; a strong peak at 1290 cm^{-1} was attributed to $\nu_{(Ph-O)}$. $\nu_{(C=N)}$, $\nu_{asym(COO)}$, and $\nu_{sym(COO)}$ were very similar to those of **J**, indicating no significant change in the original coordination of these groups upon supporting. On the other hand, the $\nu_{(Ph-O)}$ peak shifted to 1391 cm^{-1}, indicating the structural reconstruction of the Ph–O coordination to produce a Ph–OH moiety that was promoted by proton transfer from Si–OH. A small difference between $\nu_{asym(COO)}$ and $\nu_{sym(COO)}$ (230 cm^{-1}) indicated the delocalization of electron density on the C=O bond to O–CO, which made a hydrogen bond with a Ph–OH group of an adjacent V complex.

Figures 5a and 5b show ESR spectra for the SiO_2-supported V complex (**K**) in the presence and absence of O_2 measured at 6 K. A broad peak overlapped hyperfine signals attributed to d^1 configuration of the V=O complex and it widely increased after exposure to O_2 (Figure 5b). An appearance of a half-band signal was also detected after the O_2 exposure (Figure 5a), indicating the magnetic interaction between two V complexes on the surface. Similar tendencies were observed after the coordination of 2-naphthol as shown in Figures 5c and 5d.

The interatomic distance of V–V in the V dimer was estimated by the ESR spectra. The relative intensity of the forbidden half-field transition ($|\Delta M_s| = 2$) to the allowed transition ($|\Delta M_s| = 1$) was relative to r^{-6} (r: interatomic distance of V–V).[95] The distance of the two V centers was estimated to be 0.40 ± 0.05 nm, which was suitable for the activation of O_2 between the two V sites. After evacuation of the O_2-adsorbed sample, the intensity returned to the original value and the change in the ESR signal occurs reversibly, which indicated the reversible adsorption of O_2 molecules on the V dimer (**K**). The broad signal and the behavior of oxygen molecules were

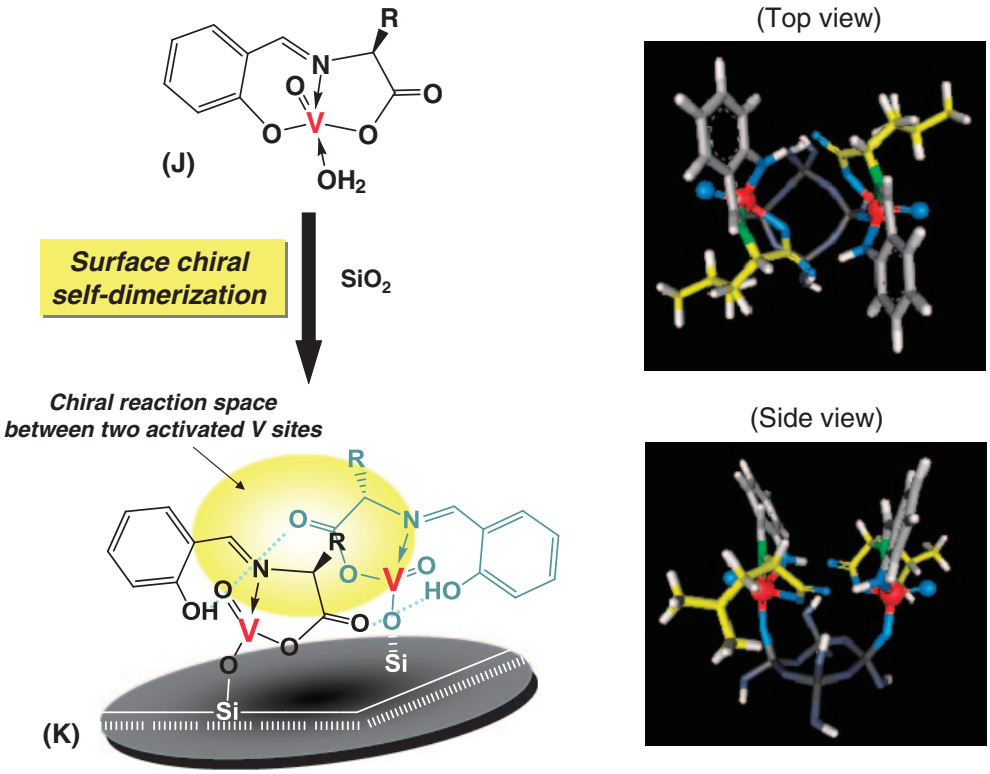

Figure 4. Chiral self-dimerization of V Schiff-base complex on SiO_2 and modeled structures of chiral self-dimerized V–L-leucine complex (**K**) by DFT calculations (top view and side view).

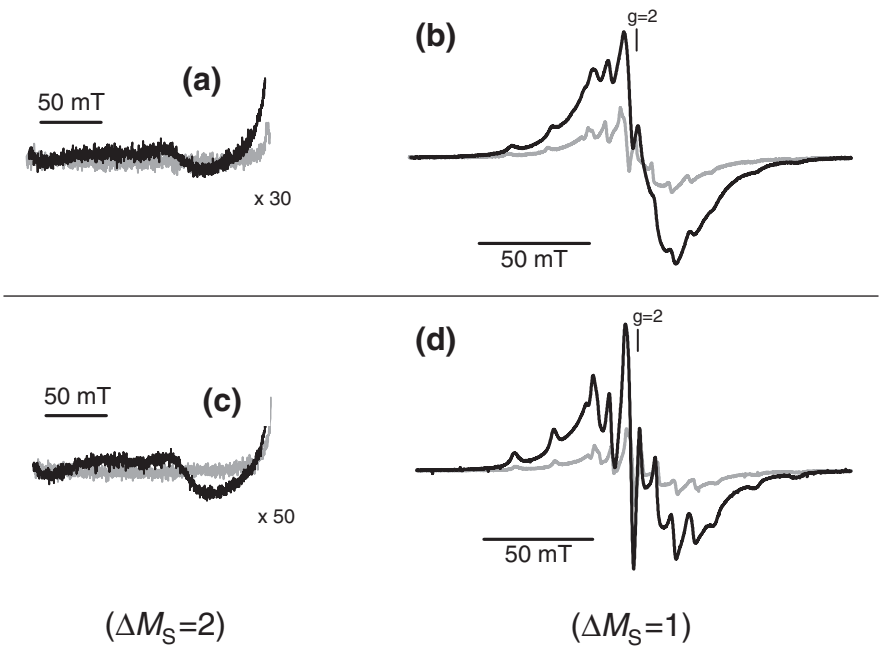

Figure 5. ESR spectra for the supported V–L-leucine dimer (V 3.4 wt %) at 6 K before (a and b) and after (c and d) the coordination of 2-naphthol. (a) and (c): half-band signal, (b) and (d): main signal.

observed in the range of V loading 0.3–3.4 wt %, indicating that the chiral self-dimerization of the V precursors (**J**) occurred independent of V loading on the SiO_2 surface.[72,73]

The chiral self-dimerized V complexes (**K**) were active for the oxidative coupling of 2-naphthol, while the homogeneous V precursors (**J**) were inactive under aerobic conditions as shown in Table 1. In toluene, 96% conversion with 100% BINOL selectivity and 99% conversion with 100% BINOL selectivity were observed on SiO_2-supported V–L-leucine-derived dimer and SiO_2-supported V–L-valine-derived dimer, respectively. On the other hand, γ-Al_2O_3 and TiO_2 were not suitable for supports for the immobilization of the V complex

Table 1. Catalytic Performance of Homogeneous (**J**) and Heterogeneous (**K**) V Catalysts for the Oxidative Coupling of 2-Naphthol[a)]

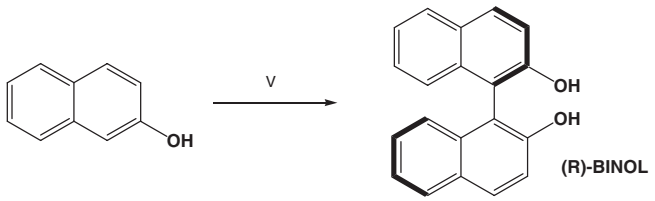

Catalyst–ligand[b)]	T/K	Time/d	Solvent	Conv./%	Selec./%	% ee (*R*)
(**J**) V–L (precursor)[c)]	293	3	$CHCl_3$	15	73	8
V–L/Al_2O_3 1.7 wt %	293	5	$CHCl_3$	69	53	−2
V–L/TiO_2 0.8 wt %	293	5	$CHCl_3$	52	0	—
(**K**) V–L/SiO_2 0.3 wt %	263	5	$CHCl_3$	9	100	54
(**K**) V–I/SiO_2 0.3 wt %	263	5	$CHCl_3$	6	100	51
(**K**) V–F/SiO_2 0.3 wt %	263	5	$CHCl_3$	9	100	56
(**K**) V–L/SiO_2 0.3 wt %	293	5	Toluene	96	100	13
(**K**) V–L/SiO_2 0.3 wt %	263	5	Toluene	11	100	32
(**K**) V–L/SiO_2 0.3 wt %[d)]	263	5	Toluene	10	100	33
(**K**) V–L/SiO_2 0.8 wt %	263	5	Toluene	33	100	39
(**K**) V–L/SiO_2 1.6 wt %	263	5	Toluene	42	100	48
(**K**) V–L/SiO_2 3.4 wt %	263	5	Toluene	93	100	90
(**K**) V–L/SiO_2 3.4 wt %[d)]	263	5	Toluene	91	100	89

a) V dimer/2-naphthol was 1/36 and 100 mg of supported catalysts were used in 5 mL of toluene. b) L: L-leucine, V: L-valine, I: L-isoleucine, and F: L-phenylalanine. c) Homogeneous reaction and chlorotrimethylsilane was added. d) Reused.

(**J**), leading to low BINOL selectivity (Table 1). It is suggested that the chiral self-dimerization did not proceed on the surfaces of γ-Al_2O_3 and TiO_2.

There were no significant differences in the performances between the V-dimer catalysts derived from L-isoleucine (51% ee), L-leucine (54% ee), and L-phenylalanine (56% ee) in $CHCl_3$ and the enantioselectivity was not affected by the chiral alkyl groups of the Schiff-base ligands. The two alkyl groups (R–) of the Schiff-base ligands overhung outside the V dimer (**K**) and seemingly they did not affect the enantioselectivity for the coupling reaction between the two V sites.

When the loading of the supported V complex (**K**) increased on the surface of SiO_2, the enantioselectivity dramatically changed in the range of V loading 0.3–3.4 wt % as shown in Table 1. Accompanied by an increase in V loading 0.3, 0.8, 1.6, and 3.4 wt %, the enantioselectivity dramatically increased to 32, 39, 48, and 90% ee, respectively. The 3.4 wt % V–L-leucine catalyst exhibited the highest 90% ee. From the estimation of the cross section of the V precursor, the V loading of 3.4 wt % corresponded to full coverage of the V complex on the SiO_2 surface, where the configuration and reaction environment of the V dimer on the surface were suggested to be regulated rigidly for the achievement of higher enantioselectivity compared to the lower V loadings.

The enantioselectivity of the oxidative coupling was determined by the chiral reaction space between the two V sites on the surface rather than the chirality of the Schiff-base ligands themselves. The chirality of the ligands sterically affected the chiral self-dimerization of V complexes on the surface. Increase in V loading achieved the higher regulation of mobility of the assembled V species on the surfaces, resulting in the high enantioselectivity (90% ee) at 93% conversion on the V 3.4 wt % catalyst compared to the case of the V 0.3 wt % catalyst with the same V local-coordination structure. The selective transformation of metal coordination at the SiO_2 surface, chiral self-dimerization, produces a unique reaction space for the oxidative coupling of 2-naphthol.[72,73]

1.5 Surface Molecular Imprinting of Supported Metal Complexes for Tailor-Made Design of Shape-Selective Reaction Space on Oxide Surfaces. Molecular imprinting is a technique to create a cavity with a shape of a particular molecule (template) in a polymer matrix.[96–112] Organic or inorganic monomer is polymerized in the presence of a target molecule (template) and a cavity with a similar shape to the template is prepared after the extraction of the template from the polymer matrix. Molecular imprinting has been applied to receptors, chromatographic separation, fine chemical sensing, and catalysis.[11,28,29,113–130]

In 2002, we proposed the design of a molecularly-imprinted metal-complex catalyst on an oxide surface, whose ligand was used as a template.[11,28,29,126–130] Surface-matrix overlayers were stacked on an oxide surface attaching a metal complex whose ligand was a template, and then the coordinating template was selectively released from the supported metal complex, resulting in forming a shape-selective reaction space (molecularly-imprinted cavity) on the active metal center. Molecular imprinting of a supported metal complex provides the following five factors for the regulation of selective catalysis, (I) conformation of ligands coordinating to a metal center, (II) orientation of a vacant site (cavity) on the metal center, (III) molecularly-imprinted cavity with a similar shape to a template, (IV) architecture of the cavity wall, and (V) a micropore structure in the surface-matrix overlayers to stabilize the active metal species.

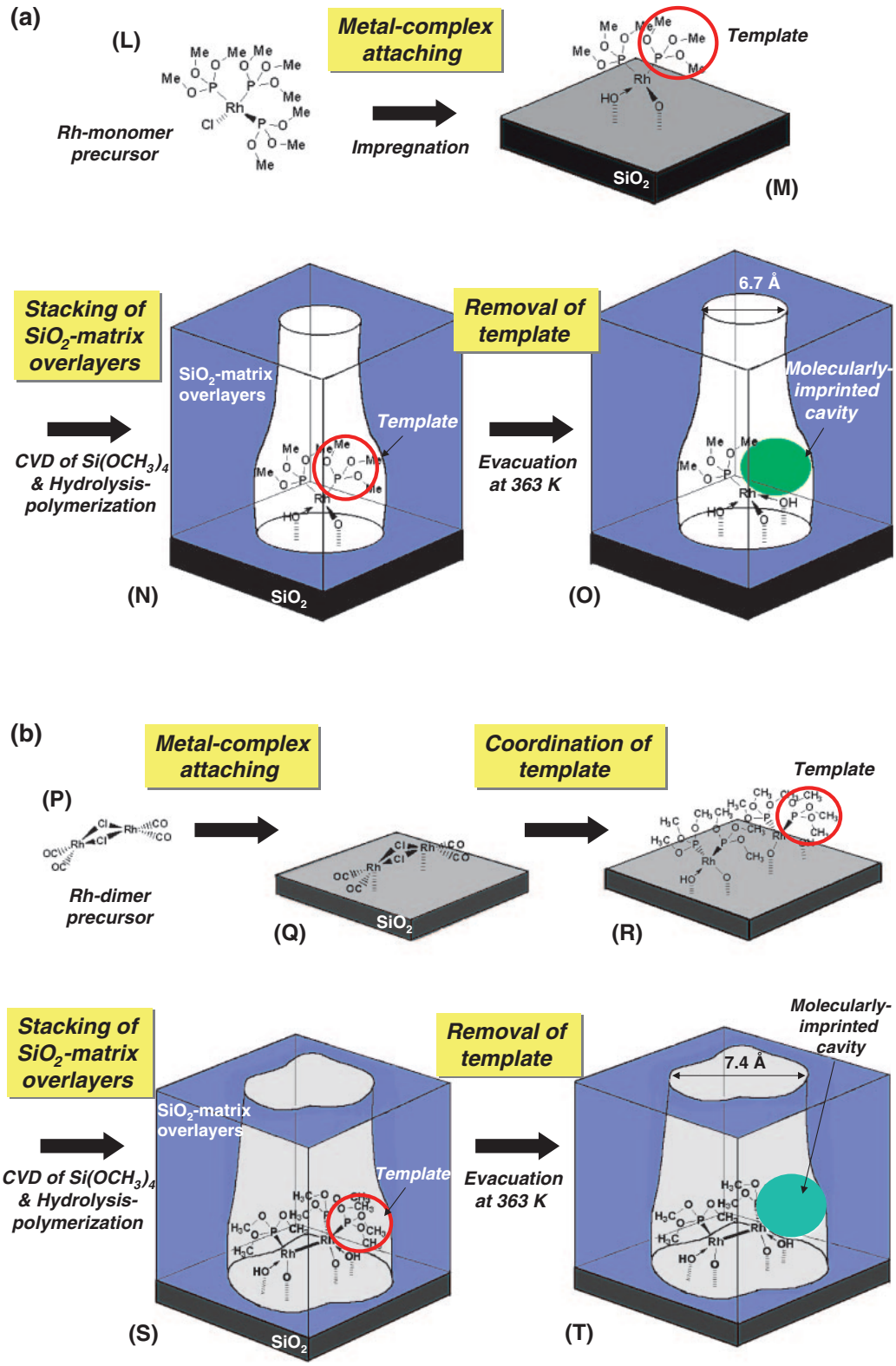

Figure 6. Preparation routes of a molecularly-imprinted Rh-monomer catalyst (a) and a molecularly-imprinted Rh-dimer catalyst (b) on SiO_2 surfaces.

Figure 6 shows the preparation routes of a molecularly imprinted Rh monomer catalyst (a) and a molecularly imprinted Rh dimer catalyst (b) on SiO_2 surfaces, whose $P(OCH_3)_3$ ligand is used as a template for hydrogenation of 3-ethyl-2-pentene.[127–129] The structure of $P(OCH_3)_3$ coordinated to Rh is regarded as a template for a half-hydrogenated species of 3-ethyl-2-pentene. The rate-determining step of alkene hydrogenation is suggested to be a half-hydrogenation step so that

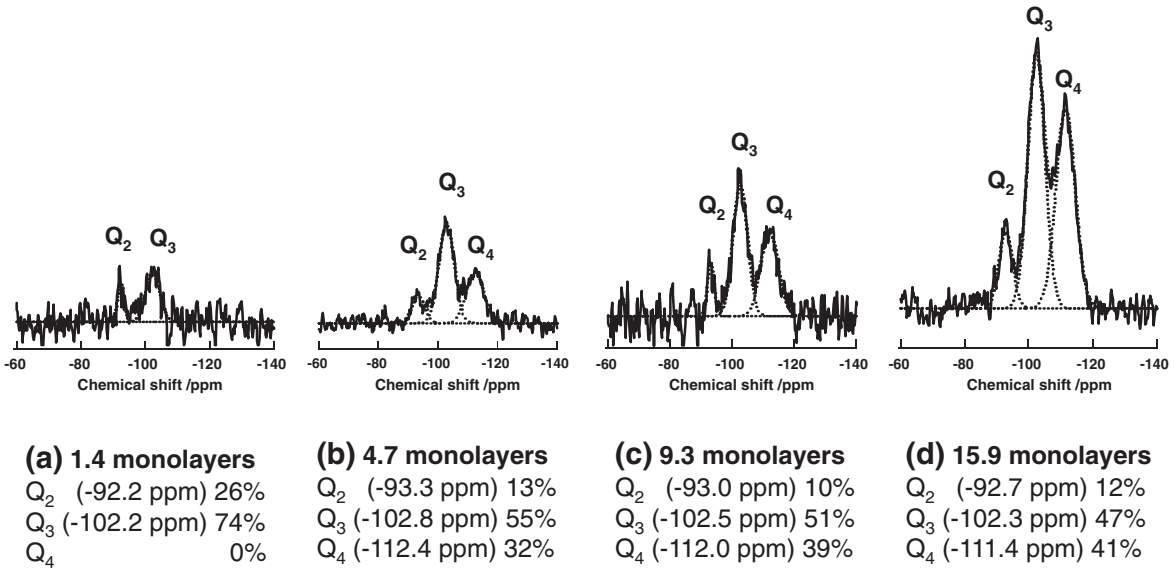

Figure 7. ^{29}Si solid-state NMR difference spectra for surface SiO_2-matrix overlayers on the molecularly-imprinted Rh-monomer catalysts on SiO_2. (a) 1.4 monolayers, (b) 4.7 monolayers, (c) 9.3 monolayers, and (d) 15.9 monolayers.

the molecular imprinting of $P(OCH_3)_3$ can produce a shape-selective cavity designed for a key intermediate structure for the hydrogenation of 3-ethyl-2-pentene.

A Rh-monomer precursor $[RhCl\{P(OCH_3)_3\}_3]$ (**L**) was attached to a SiO_2 surface (**M**), leading a $Rh\{P(OCH_3)_2\}$ monomer via bidentate immobilization as shown in Figure 6a. Surface SiO_2-matrix overlayers were prepared by chemical vapor deposition (CVD) of $Si(OCH_3)_4$ and H_2O and subsequent hydrolysis–polymerization of them on the SiO_2 surface. One of the $P(OCH_3)_3$ ligands was then selectively eliminated from the supported Rh monomer (**M**) and a molecularly-imprinted cavity with a similar shape to $P(OCH_3)_3$ was produced on the active Rh center behind the template $P(OCH_3)_3$ (**O**).[129]

$Si(OCH_3)_4$ with methoxy groups was utilized for the molecular imprinting of the $[Rh(P(OCH_3)_3)_2]$ complex, which can positively interact with $Si(OCH_3)_4$ during polymerization. Figure 7 shows ^{29}Si solid-state NMR difference spectra for the surface SiO_2-matrix overlayers in the loading range of 1.4–15.9 monolayers, indicating layer-by-layer stacking of the SiO_2-matrix overlayers on the SiO_2 surface. 1.4 monolayers of the SiO_2-matrix overlayers did not contain Q_4 bulk Si species ($Si–(OSi)_4$) as shown in Figure 7a. The absence of Q_4 in the 1.4-monolayer SiO_2 matrix suggestes that the formation of the SiO_2-matrix overlayers proceeded layer-by-layer by the reaction between surface Si–OH group and $Si(OCH_3)_4$, not by that between two $Si(OCH_3)_4$ molecules irrelevant to the SiO_2 surface. 50% of Si species were Q_3 ($Si–(OH)(OSi)_3$) in the SiO_2-matrix between the monolayer range of 4.7 to 15.9, indicating that the surface-matrix overlayers possessed many Si–OH groups like xerogels.[129]

A Rh-dimer catalyst was prepared in a similar manner by using $[Rh_2Cl_2(CO)_4]$ (**P**) as a precursor. After the coordination of $P(OCH_3)_3$ to a SiO_2-attached $[Rh_2Cl_2(CO)_4]$ (**Q**), the Rh dimer structure was converted to two Rh monomers with two $P(OCH_3)_3$ ligands on each Rh site as shown in Figure 6b (**R**). Rh K-edge EXAFS revealed that there was no direct interaction between the two Rh sites and two Rh–P bonds at 0.224 nm and two Rh–O interactions at 0.203 nm were observed. Surface SiO_2-matrix overlayers were stacked by the hydrolysis–polymerization and the final evacuation at 363 K promoted the elimination of one of the $P(OCH_3)_3$ ligands, leading a Rh dimer with a direct Rh–Rh bond at 0.268 nm (**T**).[127,128]

The mechanism of the Rh-dimer formation was investigated by DFT calculations.[128] Steric hindrance between four $P(OCH_3)_3$ ligands on the Rh-monomer pair $[Rh\{P(OCH_3)_3\}_2]$ (**R**) was enhanced during the hydrolysis–polymerization, and one of the $P(OCH_3)_3$ ligands was eliminated from one of the two Rh monomers. The Rh site losing the $P(OCH_3)_3$ ligand was presumed to react with another Rh monomer to stabilize its unsaturated structure to form $[Rh_2\{P(OCH_3)_3\}_3]$ (**S**). The final evacuation after stacking of the SiO_2-matrix overlayers promoted the further elimination of another $P(OCH_3)_3$ ligand on the Rh site with two $P(OCH_3)_3$ ligands. The last elimination of $P(OCH_3)_3$ produced a molecularly-imprinted cavity with a similar shape to $P(OCH_3)_3$ on the Rh dimer $[Rh_2\{P(OCH_3)_3\}_2]$ (**T**). The pore size of the molecularly-imprinted Rh-dimer catalyst (**T**) was estimated to be 0.74 nm in diameter by N_2-adsorption measurements at 77 K.

Table 2 shows steady-state reaction rates (TOFs (turnover frequencies)) of alkene hydrogenation at 348 K on the supported and molecularly-imprinted Rh catalysts (**M**, **O**, **R**, and **T**). Both supported Rh catalysts (**M** and **R**) exhibited catalytic activities under similar reaction conditions, while $[RhCl\{P(OCH_3)_3\}_3]$ (**L**) and $[Rh_2Cl_2(CO)_4]$ (**P**) in homogeneous phases were inactive for the hydrogenation. Furthermore, the molecularly-imprinted Rh catalysts (**O** and **T**) were more active than the supported catalysts as shown in Table 2. It is to be noted that molecular imprinting of a supported metal complex produces not only a shape-selective imprinted cavity but also unsaturated active metal centers behind the template. Indeed, the molecularly imprinted Rh dimer (**T**) was quite active for the hydrogenation and the catalytic activity of 2-pentene hydrogenation was enhanced 51-fold after the molecular imprinting.

Table 2. TOFs (Turnover Frequencies) on the Supported and Imprinted Rh Catalysts (1st Row: Rh Dimer (**R** and **T**) and 2nd Row: Rh Monomer (**M** and **O**)), Ratios of TOFs (TOF on Each Imprinted Catalyst/TOF on Corresponding Supported Catalyst), and Activation Energies E_a/kJ mol^{-1} and Activation Entropy ΔS/J K^{-1} mol^{-1} for the Catalytic Hydrogenation of Alkenes at 348 K

Reactant	Supported TOF/s^{-1}	Imprinted TOF/s^{-1}	Ratio of TOFs[a)]	Supported		Imprinted	
				E_a	ΔS	E_a	ΔS
(1) 2-Pentene	1.3×10^{-3}	6.6×10^{-2}	51	34	−205	26	−195
	1.3×10^{-3}	1.4×10^{-2}	11	35	−202	33	−188
(2) 3-Methyl-2-pentene	7.0×10^{-5}	3.6×10^{-3}	51	44	−200	43	−170
	8.3×10^{-5}	1.1×10^{-3}	13	42	−205	38	−195
(3) 4-Methyl-2-pentene	1.3×10^{-4}	5.9×10^{-3}	45	40	−207	40	−175
	1.6×10^{-4}	1.1×10^{-3}	7	38	−211	41	−186
(4) 3-Ethyl-2-pentene	4.4×10^{-5}	1.5×10^{-3}	35	42	−210	39	−189
	3.5×10^{-5}	1.2×10^{-4}	3	43	−209	11	−291
(5) 4-Methyl-2-hexene	6.8×10^{-5}	9.6×10^{-4}	14	40	−212	10	−276
	5.1×10^{-5}	1.2×10^{-4}	2	43	−206	9	−296
(6) 2-Octene	3.0×10^{-3}	3.0×10^{-2}	10	28	−215	7	−257
	3.1×10^{-3}	8.8×10^{-3}	3	29	−212	10	−259

a) Ratio of TOFs: TOF of the imprinted Rh-dimer (**T**)/Rh-monomer (**O**) catalyst/TOF of the supported Rh-dimer (**R**)/Rh-monomer (**M**) catalyst.

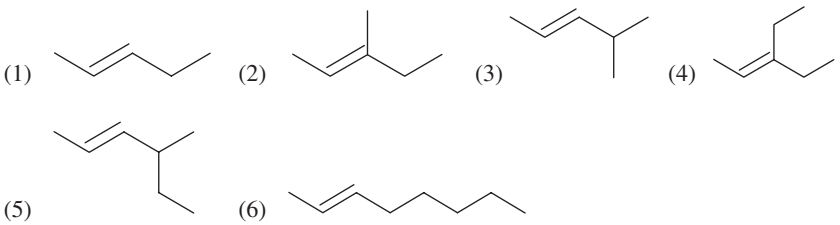

The ratios of TOFs, which correspond to be the degree of enhancement of the catalytic activity, were significantly different between 6 alkenes with different shapes as shown in Table 2. The ratios of TOFs of 2-pentene hydrogenation were 51 and 11 on the Rh-dimer and Rh-monomer catalysts, respectively, while those of 2-octene were 10 and 3. Hydrogenation of alkenes with different shapes from the template was significantly suppressed on the molecularly-imprinted Rh catalysts.

Activation energy and entropy also indicated shape-selective behavior on the molecularly-imprinted Rh catalysts. A large decrease in E_a and ΔS for 3-ethyl-2-pentene hydrogenation was observed on the molecularly-imprinted Rh-monomer catalyst (**O**). Decreases in the ratio of TOF, E_a and ΔS revealed that the coordination of 3-ethyl-2-pentene was suppressed on the Rh site and the rate-determining of the hydrogenation was shifted from the half-hydrogenated process to the coordination of alkene to Rh. The comparison between 4-methyl-2-pentene and 4-methyl-2-hexene indicated that the molecularly-imprinted Rh catalysts could discriminate the existence of a methyl group from a simple alkene without any functional groups.[127–129]

Fine shape-selectivity on the molecularly-imprinted Rh catalysts was achieved by not only the cavity with a similar shape to the template but also coordination of the supported Rh complexes and the wall of the surface-matrix overlayers. Unsaturated active metal site, molecularly imprinted space, metal coordination, and surface-matrix overlayers were integrated on the surface to achieve shape selective catalysis. Molecular imprinting of supported metal complexes is promising for tailor-made design of shape-selective reaction space on heterogeneous catalyst surfaces.

2. Creation of Novel Metal Clusters by Chemical Vapor Deposition and Their In Situ Characterization

Metal clusters often exhibit unique catalytic performance which cannot be observed on mononuclear metal compounds.[31,131] In this chapter, the structures and catalytic performance of metal-cluster catalysts prepared by CVD (chemical vapor deposition), which can produce uniform metal structures on oxide surfaces.[132] In situ characterization of the metal-cluster catalysts prepared by CVD revealed essences of catalysis and relationships between catalyst structure and reactivity.[133–136]

2.1 γ-Al_2O_3-Supported Co Tetramer for the Reduction of NO with CO. Understanding of the origin and mechanism of the activation and regulation of adsorbed molecules and reaction intermediates on catalyst surfaces is a long-term challenge to be addressed. New concepts for catalysis are conceived by understanding the surface events on catalysts and the characteristic features of catalysis based on the construction of novel single-site reaction surfaces.[3,137–141] Stepwise preparation of single-site catalyst surfaces in a controllable manner has been performed by attaching organic and inorganic metal complexes on oxide surfaces.

A Co-tetramer catalyst on γ-Al_2O_3 prepared by CVD provided a new aspect of surface catalytic reactions assisted by gas-phase molecules. Gas-phase CO molecules undetectable

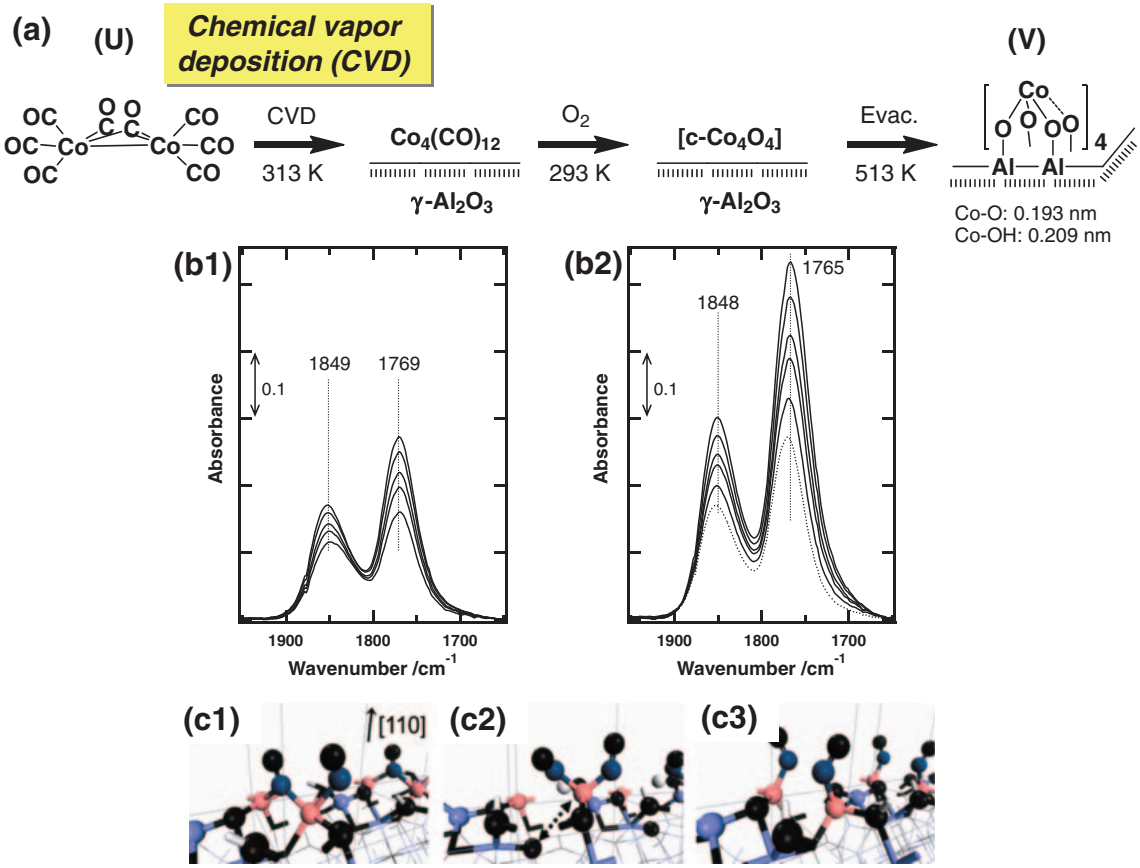

Figure 8. (a) Preparation steps of a γ-Al_2O_3-supported Co^{2+}-ensemble (Co tetramer) catalyst for the reduction of NO with CO (NO–CO reaction). (b) ν_{CO} FT-IR spectra during NO adsorption on the Co^{2+}-ensemble catalyst at 443 K. (b1) NO 5.3 kPa; 1, 2, 3, 5, and 20 min. (b2) NO 5.3 kPa, CO 5.3 kPa; 1, 3, 5, 10, and 20 min. Dotted line in (b2) represents the spectrum of (b1) at 20 min in the absence of CO. (c) Structures of dinitrosyl species on the Co^{2+}-ensemble catalyst on a γ-Al_2O_3 model surface calculated by DFT. (c1) *geminal*, (c2) *geminal*, and (c3) mononitrosyl species. Pink: Co, dark blue: N, and black O (NO).

at the surface can largely influence the amount and reactivity of strongly adsorbed NO species on the surfaces.[133,142–144] Very weakly adsorbed molecules are usually difficult to supply with driving energies for the activation of adsorbed reaction intermediates and catalytic reactions, and the collision energy of gas-phase molecules does not contribute to increase the amount and reactivity of adsorbed species either. In situ characterization has revealed the mechanism and details of this phenomenon, which has provided an essence of catalysis in a wide range of catalytic systems.[133]

γ-Al_2O_3-supported Co-tetramer catalyst (**V**) was prepared by CVD of $[Co_2(CO)_8]$ (**U**) as shown in Figure 8a. Sublimed $[Co_2(CO)_8]$ (**U**) was reacted with γ-Al_2O_3, forming a Co tetramer $[Co_4(CO)_{12}]$.[145] Subsequent oxidation and evacuation at 513 K provided divalent Co tetramer $[CoO]_4/\gamma$-Al_2O_3 (**V**) with trigonally-distorted tetragonal symmetry with Co–O bonds at 0.193 nm and Co–OH bonds at 0.209 nm. Four Co^{2+} species were believed to be supported as an ensemble structure chemically attached on the γ-Al_2O_3 surface (**V**) as illustrated in Figure 8a because the attachment proceeded via $[Co_4(CO)_{12}]$. There was no direct Co–Co bonding on the supported Co^{2+}-ensemble catalyst (**V**) but two Co atoms in a Co ensemble cooperated during the catalytic NO reduction mentioned later.[133]

The supported Co^{2+} ensembles (**V**) strongly adsorb NO as characterized by in situ FT-IR. Figure 8b shows a series of in situ FT-IR spectra in the ν_{NO} region during the adsorption of NO at 443 K in the absence (b1) and presence (b2) of gas-phase CO. Two peaks of 1849 and 1769 cm^{-1} (Figure 8b1) were attributed to symmetric and asymmetric stretching vibrations (ν_{NOsym} and ν_{NOasym}) of dinitrosyl species, respectively, as suggested by the spectrum of a mixture of ^{14}NO and ^{15}NO. The intensities of these two peaks increased with adsorption time and were saturated after 20 min of NO exposure as shown in Figure 8b1.

Interestingly, the addition of CO into the gas-phase of NO dramatically increased the amount of adsorbed NO on the Co^{2+}-ensemble catalyst (**V**) (Figure 8b2). The number of adsorbed NO in the absence of CO was 0.18 per Co and that in the presence of CO was 0.35 per Co. The positions of the ν_{NOsym} and ν_{NOasym} peaks were slightly red-shifted from 1849 to 1848 cm^{-1} and from 1769 to 1765 cm^{-1}, respectively. It is to be noted that the adsorption of CO on the surface at 373–473 K was undetectable volumetrically and spectroscopically irrespective of the large effects on the NO adsorption. At 298 K, a small peak of ν_{CO} was observed at 2160 cm^{-1}, indicating that CO was very weakly adsorbed on the surface, but there was no peak at catalytic reaction temperatures.

The structural models of the dimeric Co species for NO adsorption and catalysis were proposed by first-principles DFT calculations and two Co^{2+} ions on γ-Al_2O_3(110) surface were supported adjacently to each other in a tetrahedral symmetry.[146,147] The DFT calculations revealed that there were three structures of dinitrisyl adsorption, two *geminal* dinitrosyl species (NO–Co–NO) (Figures 8c1 and 8c2) and a pair of two mononitrosyls on each of the adjacent two Co^{2+} ions (two NO–Co) (Figure 8c3), whose adsorption energies were 1.89, 2.28, and 2.71 eV, respectively. The coupled two mononitrosyls on the Co-dimer unit (c3), whose N atoms interacted with each other at a N–N distance of 0.251 nm, was suggested to have symmetric and antisymmetric NO stretching vibration modes similar to the coupled vibration modes observed with *geminal* dinitrosyl species. The unoccupied d orbitals of the adjacent Co^{2+} ions were directed to each other, and this specific orientation enabled the two NO adsorbates in the mononitrosyls to couple with each other through an adsorbate–adsorbate interaction, showing similar ν_{NOsym} and ν_{NOasym} peaks to the coupled peaks for *geminal* species. Further in situ characterization and DFT calculations suggested the detail mechanism of the surface events by spectator CO: the mononitrosyl species (c3) and a *geminal* dinitrosyl species (c1) were formed by first adsorption of NO and spectator CO produced another *geminal* dinitrosyl species (c2), which was more stable than (c1).[133]

The γ-Al_2O_3-supported Co-ensemble catalyst (**V**) was tremendously active for the catalytic reduction of NO with CO and the equivalent amounts of N_2O and CO_2 were formed at 373–473 K. At higher temperatures than 473 K, N_2O was further converted to N_2 as complete reduction of NO: $2NO + CO \rightarrow N_2O + CO_2$ and $N_2O + CO \rightarrow N_2 + CO_2$. At 773 K, adsorbed dinitrosyl NO on the Co^{2+}-ensemble catalyst (**V**) did not produce N_2O under vacuum, while the addition of gas-phase CO brought about rapid N_2O formation, which was complete within a few minutes. On the other hand, the formation of N_2O on the dinitrosyl species (c2) after the exposure to CO was slow. It was indicated that dinitrosyl species produced by adsorption of NO were active for the N_2O formation, while gas-phase CO rapidly produced N_2O by the catalytic reaction with the active NO species but simultaneously produces less reactive NO species (c2). The DFT calculations also indicated that the both *geminal* dinitrosyl species (c1) and (c2) were inactive for N_2O formation in both the presence and absence of CO, and only the mononitrosyl species (c3) transformed to N_2O by CO.

The mechanism for catalytic NO–CO reactions on many catalysts has been simply written as a slow conversion, $2NO \rightarrow N_2O + O(ad)$, followed by fast reaction of the O(ad) with CO to form CO_2. However, the fact that the rate of the NO–CO reaction was much higher than that of NO alone demonstrated that the usual reaction mechanism was not valid for the Co^{2+}-ensemble/γ-Al_2O_3 catalyst (**V**). It was found that a reaction intermediate was profoundly influenced by the ambient CO gas undetectable at the catalyst surface and surface-undetectable gas-phase CO molecules opened a new reaction path for the adsorbed dinitrosyl species. The DFT calculations indicated that the pair of mononitrosyl species (c3) reacts preferable with gas-phase CO by the Eley–Rideal mechanism and the rate-limiting step in the reaction had much wider reactive window than typical ER reactions. The high reactivity of the Co^{2+}-ensemble catalyst (**V**) was attributed to the mononitrosyl species (c3), where the unoccupied d orbitals of the two adjacent Co^{2+} ions were directed to each other, and hence the NO molecules adsorbed on each of the adjacent Co^{2+} ions with the opposed orientation. The two adjacent NO molecules showed coupled vibration modes and easy N–N bond formation assisted by gas-phase CO through the $2\pi^*$–$2\pi^*$ bonding. The concept of surface catalytic reactions assisted by weakly adsorbed or undetectable gas-phase molecules at the surface documents an origin of catalysis by the active surface.[133]

2.2 Zeolite-Supported Re Cluster for Direct Phenol Synthesis from Benzene and O_2. Phenol is the major source of Bakelite and phenol resins, which are utilized in many commodities throughout the world. The industrial demand for phenol has increased every year and its production now exceeds 9.1 megatons per year and 94% of the world-wide phenol production has been achieved by a well-known three step process from cumene. Benzene and propene are converted to cumene, and cumene hydroperoxide is produced by auto-oxidation. Finally, the decomposition of cumene hydroperoxide using surfuric acid produces phenol and stoichiometric acetone. Direct phenol synthesis from benzene in a one-step reaction with high phenol yield is a desirable oxidation processes, however there has been no efficient catalyst to achieve high benzene conversion and high phenol selectivity.

Many oxidants have been utilized for direct phenol synthesis from benzene, for example, O_2,[148–153] H_2O_2,[154–162] N_2O,[163–172] $H_2 + O_2$,[173,174] air/CO,[175] and O_2/H_2O.[176] Liquid-phase oxidation reactions of benzene with molecular oxygen have been reported on an iron-heteropolyacid catalyst and a CuO/Al_2O_3 catalyst with ascorbic acid as a reducing reagent.[148,149] A Cu/ZSHM-5 catalyst showed a maximum phenol selectivity of 60% with a phenol yield of 1.2% at 673 K.[150] However, the selective oxidation of benzene using O_2 was nominated as one of the ten most difficult challenges in catalysis[177–179] and indeed there have been no reports on direct remarkable catalysts for phenol synthesis with performance greater than 5% benzene conversion and 50% phenol selectivity over the last 50 years.

Re is known to be an oxophilic element with various valences,[180,181] but the high sublimation propensity of Re_2O_7 prevents development of Re catalysts for oxidation.[182,183] However, supported ReO_x compounds on oxide surfaces have been reported to be different from those on unsupported ReO_x compounds.[184–187] For example, Fe_2O_3-supported ReO_x behaves as a highly selective catalyst for one-step methylal synthesis from methanol and O_2;[188–190] an octahedral ReO_x cluster in zeolite pores was active for propene oxidation/ammooxidation using NH_3.[191,192] H-ZSM-5-supported Re catalysts were found to be active for direct phenol synthesis from benzene and O_2.[134–136]

The zeolite-supported Re catalysts were prepared by CVD of CH_3ReO_3 (**W**) (Figure 9). CH_3ReO_3 easily sublimed at 313 K and entered into the pores of zeolites. Protons on Al acid sites of zeolites reacted with CH_3ReO_3 (**W**): CH_3ReO_3 (**W**) + HO–Al/Si (zeolite) $\rightarrow$ O_3–Re–O–Al/Si (**Y**) + CH_4. The stoichiometric amount of CH_4 evolved during the attachment indicated that the Re precursor (**W**) was chemically attached to H-ZSM-5 zeolite.

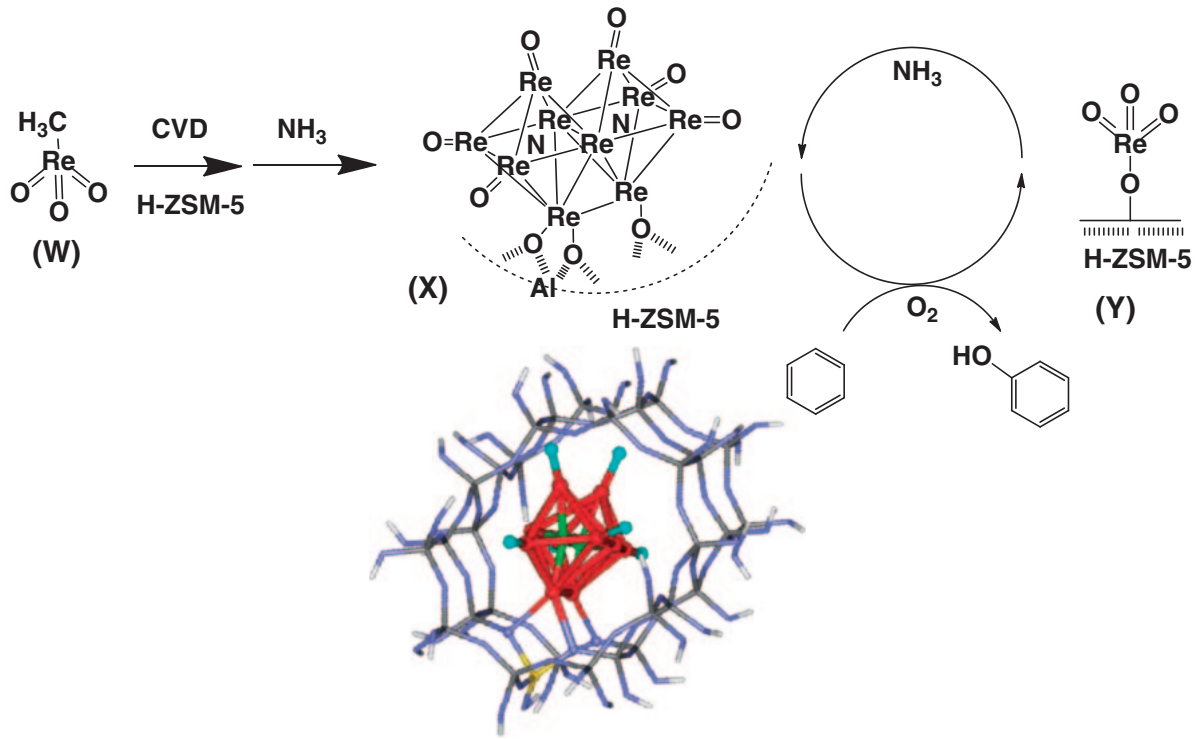

Figure 9. Structural transformations of supported Re catalyst on HZSM-5 for direct phenol synthesis from benzene and O_2. A modeled structure of the Re_{10} cluster embedded in the pore of HZSM-5 is presented.

Catalytic activity and selectivity for the phenol synthesis largely depended on the types of zeolites and the numbers of Al in zeolites. The order of phenol yields for zeolite supports was as follows: H-ZSM-5 $\gg$ H-Mordenite > H-Beta > H-USY $\geqq$ SiO_2–Al_2O_3 = γ-Al_2O_3. H-ZSM-5 has a three-dimensional pore structure with a pore size of 0.56 nm in diameter and its acidity is known to be intermediate among these zeolites. H-Mordenite and SiO_2–Al_2O_3 are stronger acids than H-ZSM-5; H-USY is a weaker acid than H-ZSM-5; H-Beta is basic. Both acidity and pore geometry of zeolite supports are important issues for the catalytic performances of zeolite-supported Re catalysts for the phenol synthesis from benzene and O_2.[136]

Both benzene conversion and phenol selectivity increased accompanied with increasing the numbers of Al sites of H-ZSM-5: H-ZSM-5 with the SiO_2/Al_2O_3 ratio of 19 (denoted as H-ZSM-5-(19)) brought about the highest phenol yield (TOF = $65.6 \times 10^{-5}\,s^{-1}$ and phenol selectivity = 87.7%) under steady-state reaction conditions in the presence of NH_3. The TOF value corresponds to 0.8% benzene conversion on a 0.6 wt%-Re catalyst, and 5.8% benzene conversion was achieved on a 2.2 wt%-Re/HZSM-5-(19) catalyst with the phenol selectivity of 82.4%.

It should be noted that NH_3 is indispensable to maintain the catalytic activity of the phenol synthesis under steady-state reaction conditions. In the absence of NH_3, neither benzene combustion nor phenol formation occur on Re/H-ZSM-5-(19) catalyst under steady-state reaction conditions. Other amine compounds such as isopropylamine or pyridine did not promote the catalytic oxidation at all, which indicates that the role of NH_3 in the catalysis is not related to basicity. Fe/ZSM-5 has been reported to be active and selective for phenol synthesis from benzene with N_2O as an oxidant,[158,159] but N_2O did not act as an active oxidant on the supported Re catalyst. Other NO_x compounds also had no effect on the phenol synthesis.[136]

Re L_I-edge and L_{III}-edge XAFS revealed that Re^{7+} monomer (**Y**) with a Re–O bond (CN = 1.3 ± 0.6) at 0.211 ± 0.002 nm and three Re=O bonds (CN = 3.5 ± 0.6) at 0.173 ± 0.001 nm was formed after the steady-state reaction. However, the Re monomer (**Y**) was inactive to a mixture of benzene and O_2 and no formation of phenol was observed at 553 K. It is to be noted that the NH_3 treatment of the Re monomer (**Y**) at 553 K remarkably changed Re structure and its catalytic activity as shown in Figure 10a. The catalytic activity dramatically increased between 40 and 60 min of the NH_3 treatment and saturated after 120 min. Phenol selectivity was constant (90.1–93.9%) during the entire NH_3 treatment.[136]

Re L_{III}-edge EXAFS revealed the structural changes in the supported Re species, whose Fourier transforms are presented in Figure 10b. After 30 min of exposure to NH_3, three chemical bonds were observed: Re=O (CN = 0.3 ± 0.3) at 0.167 ± 0.002 nm, Re–O (CN = 2.3 ± 0.4) at 0.204 ± 0.001 nm, and Re–Re (CN = 1.3 ± 0.3) at 0.278 ± 0.001 nm. Negligible catalytic activity in this stage demonstrated that small Re clusters such as dimers do not act as active species for the direct phenol synthesis from benzene and O_2. After 60 min, the CN of Re–Re bonds at 0.277 ± 0.001 nm increased to 2.8 ± 0.3, and those of Re=O bonds and Re–O/N bonds were 0.2 ± 0.2 at 0.171 ± 0.002 nm, and 2.6 ± 0.2 at 0.205 ± 0.001 nm, respectively. Assuming that a Re_6 octahedral structure is stable,[192] the CN (2.8) of the Re–Re bonds means that a part of the Re species clustered to a Re_6 octahedron framework.

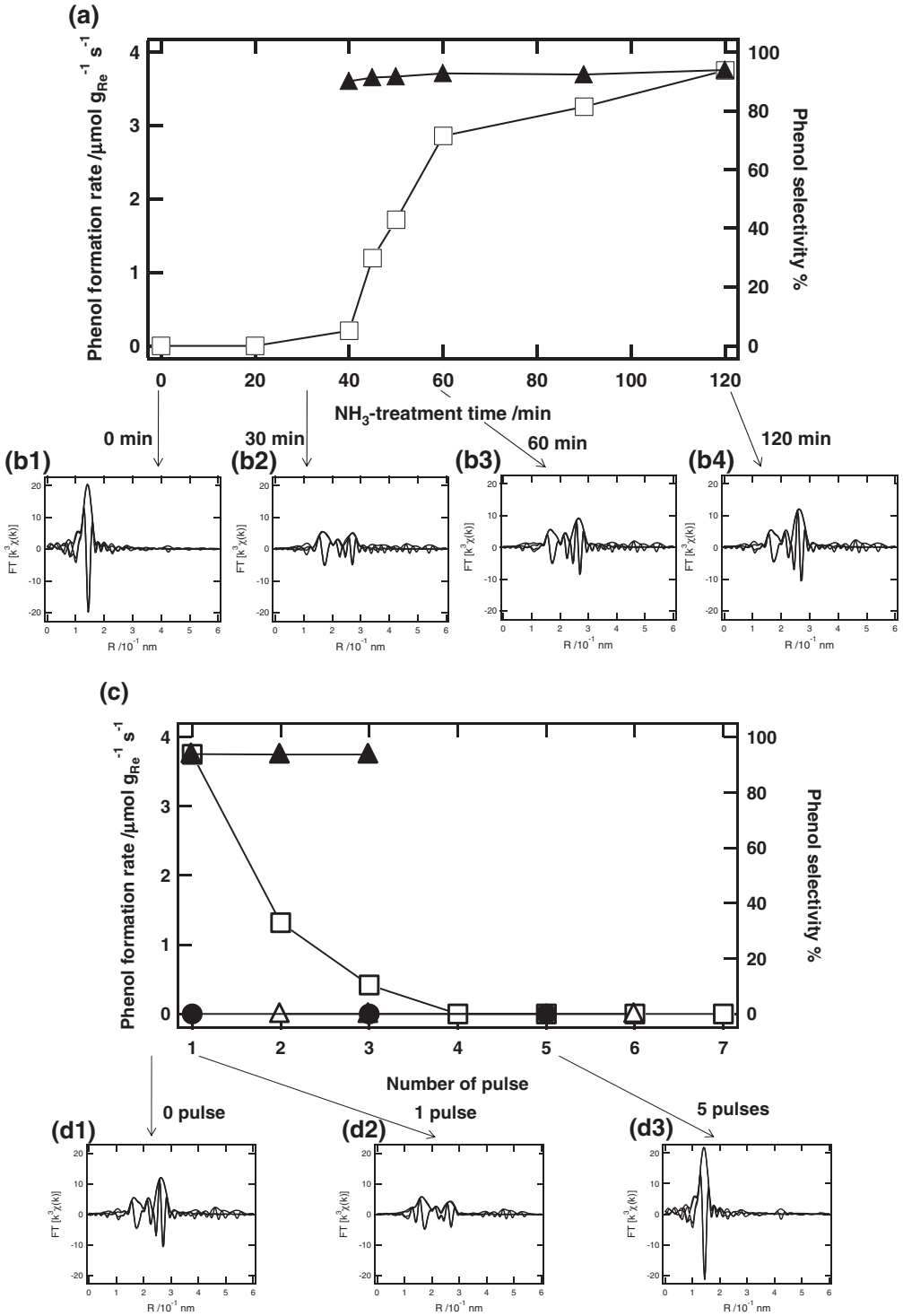

Figure 10. (a) Changes in the catalytic performance (phenol formation rate: □ and phenol selectivity: ▲) on the Re/HZSM-5-(19) catalyst by exposure to NH_3. NH_3 treatment: 553 K, NH_3–He flow (NH_3/He = 74/26 (mol %)). Catalytic reaction: pulse reaction, 553 K, catalyst = 0.1 g, pulse volume = 0.42 mL, He/O_2/benzene = 81/12/7 (mol %). (b) Re L_{III}-edge EXAFS Fourier transforms measured at 15 K during exposure to NH_3 at 0 (b1), 30 (b2), 60 (b3), and 120 min (b4). (c) The catalytic performance of pulse reactions with benzene on the Re-cluster/HZSM-5-(19) after 120-min exposure to NH_3 (phenol formation rate: △), pulse reactions with benzene and O_2 on the Re-monomer/HZSM-5-(19) after the steady-state reaction (phenol formation rate: ●), and pulse reactions with benzene and O_2 on the Re-cluster/HZSM-5-(19) after the 120-min exposure NH_3 (phenol formation rate: □ and phenol selectivity: ▲). Pulse reactions: 553 K, catalyst = 0.1 g, pulse volume = 0.42 mL, He/O_2/benzene = 81/12/7 (mol %) (in the presence of O_2) or He/O_2/benzene = 93/0/7 (mol %) (in the absence of O_2). (d) Re L_{III}-edge EXAFS Fourier transforms measured at 15 K during the pulse reactions with benzene and O_2 on the Re-cluster/HZSM-5-(19) catalyst after the 120-min NH_3 treatment. (d1) Before the pulse reaction, (d2) after the first pulse reaction, and (d3) after the fifth pulse reaction.

After 120 min, the clustering of supported Re species was complete and the Re–Re bonds finally became 5.2 ± 0.3 at 0.276 ± 0.002 nm. N_2 TPD and DFT calculations suggested a proposed structure, N-interstitial Re_{10} cluster illustrated in Figure 9 (**X**). N atoms at the edge and hollow sites of the Re cluster never stabilized the Re cluster framework with Re–Re bonds at 0.276 nm. Interstitial N drew the Re atoms of the Re_6 framework and stabilized the Re_6 octahedron. Thus NH_3 reduced the supported Re^{7+} species as a reductant and also provided N atoms to stabilize the Re_6 framework.

The Re_6 octahedron framework, which is a stable structure, can be connected together as an edge-shared structure such as the Re_{10} cluster (**X**). The formation of the edge-shared Re_{10} cluster (**X**) may be due to the structure and size of the pore of the H-ZSM-5 zeolite. The pore size of H-ZSM-5 (0.56 nm) may prohibit the further oligomerization of the Re_6 octahedron framework such as Re_{14} and Re_{18} clusters. H-ZSM-5 is suggested to play roles not only to provide the acid sites for attaching CH_3ReO_3 (**W**) but also to regulate the structure of the Re_{10} clusters. After the formation of the Re_{10} cluster on H-ZSM-5 by NH_3, a broader peak at 53.6 ppm on ^{27}Al solid-state NMR implies a positive interaction between the Al acid sites and the Re_{10} clusters inside the pore of H-ZSM-5.

Figures 10c and 10d show the performance and Fourier transforms at Re L_{III}-edge for pulse reactions of benzene and O_2 on the N-interstitial Re_{10} cluster (**X**). When a pulse of a mixture of benzene and O_2 was admitted onto the N-interstitial Re_{10} cluster (**X**), phenol was produced with the selectivity of 93.9% in the absence of NH_3. It is to be noted that the direct phenol synthesis from benzene and O_2 on the N-interstitial Re_{10} cluster (**X**) proceeds in the absence of NH_3. The pulse of benzene without O_2 did not produce phenol as shown in Figure 10c, indicating that oxygen in the Re_{10} cluster did not behave as active oxygen species.

Re L_{III}-edge EXAFS analysis after the fifth pulse reaction of benzene and O_2 revealed the formation of Re monomers with Re=O bonds ($CN = 3.7 \pm 0.2$) at 0.173 ± 0.001 nm and Re–O bond ($CN = 1.3 \pm 0.7$) at 0.213 ± 0.003 nm, which was similar to that observed after the steady-state reaction. Thus, the inactive Re monomers (**Y**) converted to the active Re_{10} cluster (**X**) by NH_3, and the Re_{10} cluster (**X**) produced phenol from benzene and O_2 accompanied by the decomposition of the Re_{10} cluster as shown in Figure 9. Hence NH_3 is indispensable to maintain catalytic activity for the phenol synthesis under steady-state reaction conditions.[136]

3. Structural Kinetics of Catalytically Active Metal Species Studied by In Situ Time-Resolved XAFS under Catalyst Working Conditions

3.1 Structural Kinetics of Supported Re_{10}-Cluster Catalyst for Direct Phenol Synthesis. Phenol synthesis proceeded via the dynamic structural changes of a catalytically active Re species.[136] The phenol synthesis occurred on the active Re_{10} cluster (**X**) supported on H-ZSM-5, but only the inactive Re monomers (**Y**) were observed after steady-state reaction. The reason of the catalyst structure–reactivity gap can be explained by the difference in the rates between the oxidation and Re-cluster formation. Phenol synthesis from benzene and O_2 on the Re cluster (**X**) was suggested to be completed for 4.4 s and the Re cluster was oxidized to the inactive ReO_4 monomers (**Y**) competitively. Under the steady-state conditions in the presence of NH_3, the population of the active Re_{10} clusters was less than 5%, which cannot be captured by in situ EXAFS under the catalytic reaction conditions.

There are two typical techniques of rapid XAFS measurements, called quick XAFS (QXAFS) and energy-dispersive XAFS (DXAFS), whose principle is presented in Figure 11.[193–198] QXAFS is obtained by rapid sweep of monochrometers (Si crystals) and energy-dispersed X-rays are used for DXAFS. White X-rays from a synchrotron reflect from an elliptically bent crystal of a polychromator and a sample at a focusing point of energy-dispersed X-rays can absorb the whole range of X-rays for a XAFS spectrum. The energy-dispersed X-rays are detected by a position sensitive detector (ex. photodiode array (PDA)) and a successive XAFS measurement can be performed.[199–211]

Figure 12a shows the series of in situ energy-dispersive XANES (DXANES) at Re L_{III}-edge measured at 553 K during the reaction of benzene and O_2 on the Re_{10} cluster catalyst on H-ZSM-5-(19) (**X**).[136] White-line intensity at Re L_{III}-edge increased accompanied by the benzene oxidation. At least three isosbestic points (10562, 10597, and 10636 eV) were observed in the series of the DXANES spectra, which indicated that the Re_{10} cluster (**X**) directly converted to the Re monomers (**Y**) without the existence of definite intermediates in this time scale. Thus, the series of the DXANES spectra can be given by the linear combination of the DXANES spectra of the initial Re_{10} cluster (**X**) and the final Re monomers (**Y**). The series of DXANES spectra were successfully fitted with the linear combination of these spectra and the sums of both coefficient parameters for the linear combination were 1.0 ± 0.005 at the full stage of the selective benzene oxidation.

Figure 12b shows the plots of the coefficient parameters of **X**, which means the concentration of the Re_{10} cluster (**X**), against reaction time. The linear plots in Figure 12b revealed that the Re_{10} cluster (**X**) disintegration was a first-order reaction. Together with the existence of isosbestic points in the Re L_{III}-edge DXANES spectra, this indicates that the first step for the oxidation reaction is the reaction between the Re_{10} cluster and O_2 followed by faster decomposition steps to the Re monomers (**Y**) in the presence of gas-phase O_2.

In general, metastable intermediate structures with low selectivity emerge during such a large structural change of metal clusters in catalysis. As a result, overall selectivity widely depends on the existence of metastable intermediates during metal-cluster disintegration. If there are some intermediate structures with low phenol selectivity, the overall phenol selectivity decreases no matter how well the initial cluster performs. For the Re/H-ZSM-5-(19) catalyst, the in situ characterization of the dynamic structural changes in the catalytically active species suggested that the following three phenomena are key factors to achieve high phenol selectivity on the Re/H-ZSM-5 catalyst: (1) there were no unfavorable intermediates during the decomposition of the active Re_{10} cluster (**X**) with O_2, (2) the Re monomer (**Y**) destination was completely inactive for the benzene oxidation, and (3) there was selective arrangement between benzene and O_2 to produce phenol on the Re_{10} clusters in the pores. The structural kinetics

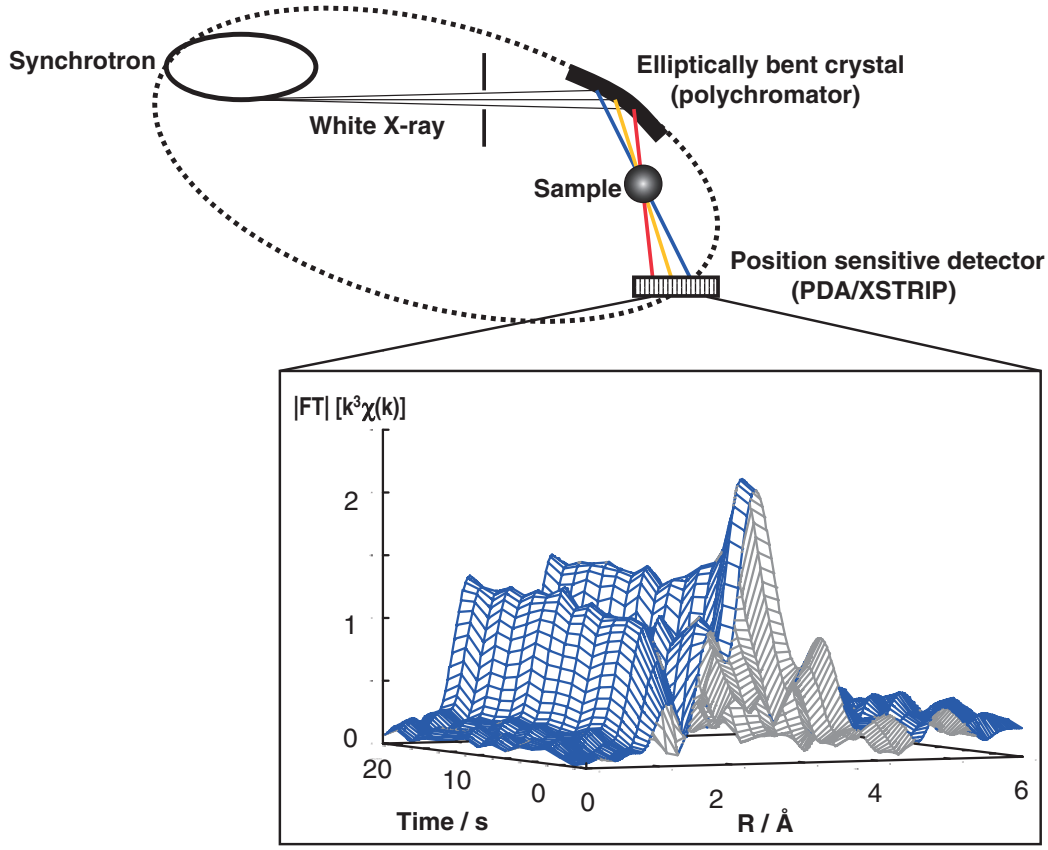

Figure 11. Principle of energy-dispersive XAFS (DXAFS) and an example of a series of DXAFS Fourier transforms.

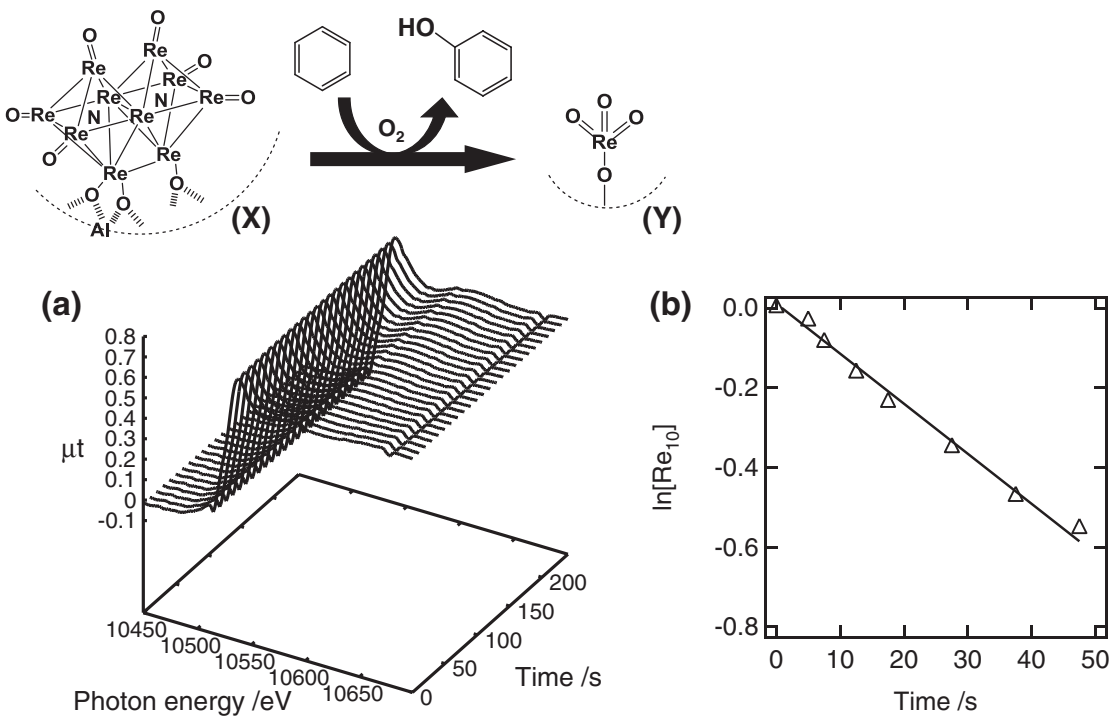

Figure 12. (a) A series of in situ time-resolved DXANES at Re L_{III}-edge of the Re-cluster/HZSM-5-(19) catalyst during the selective benzene oxidation with O_2. 553 K; $p_{O_2} = 9.7$ kPa; $p_{benzene} = 4.8$ kPa. (b) The plot of the concentration of the Re_{10} cluster (**X**) ($[Re_{10}]$) during the selective benzene oxidation at 553 K.

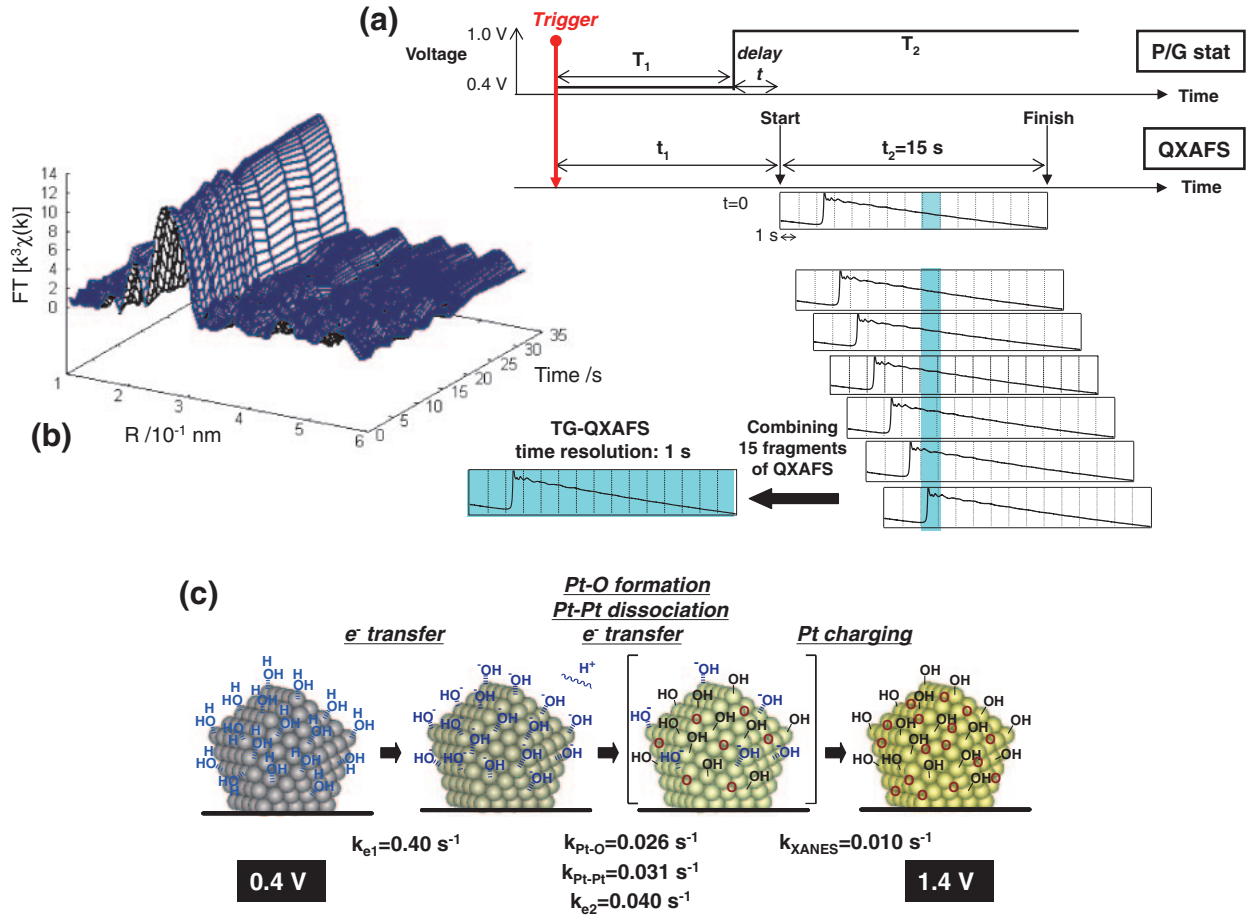

Figure 13. (a) The procedure for time-gating quick XAFS (TG-QXAFS) measurements with a time resolution of 1 s for fuel-cell operating systems. (b) A series of TG-QXAFS Fourier transforms at Pt L_{III}-edge in a Pt/C fuel-cell catalyst at 333 K for a voltage-operating process from 0.4 to 1.0 V (anode: H_2, cathode: N_2). (c) The structural models of the Pt nanoparticles suggested by in situ time-resolved QXAFS for the voltage-operating process from 0.4 to 1.4 V (anode: H_2, cathode: N_2). The subsurface oxygen atoms should reconstruct the Pt surface, but it is not shown to avoid speculation for the reconstructed structure.

of the catalytically active species under the reaction conditions provide a concrete prospect for further development of novel catalysts for the direct phenol synthesis.[136]

3.2 Reaction Dynamics of Practical Pt/C Fuel-Cell Catalysts under Fuel-Cell Operating Conditions. The high transmission of hard X-rays enables in situ measurements of XAFS under catalyst working conditions in the presence of gases and liquids. Environmentally friendly proton-exchange-membrane fuel cells (PEMFC) are considered to be a possible answer to environmental and energy problems,[212–216] however the activity and life of Pt/C cathode catalysts must be improved to make fuel-cell automobiles a reality. Wet system fuel cells present many difficulties in understanding structures of active metal catalysts under working conditions and reaction mechanisms at electrode surfaces.

Power-on and -off processes (voltage change from open-circuit voltage (*OCV* = e.g., 1.0 V) to operating voltage (e.g., 0.4 V)) with huge energy transfer are indispensable for commercial applications of fuel-cell systems. It is a serious problem that metal catalysts in PEMFC dissolve into electrolyte when such power-on and -off processes repeat.[217,218] This effect is a problem because automobiles, in particular, require continual repetition of the on/off processes with rapid changes in cell voltages to alter the car's speed.

The measurements of Quick XAFS (QXAFS) under fuel-cell operating conditions has revealed the dynamic surface events involving Pt dissolution at a Pt/C cathode surface in a fuel cell.[219–225] A new time-gating quick XAFS (TG-QXAFS) technique was developed synchronized with a potentiostat as illustrated in Figure 13a.[225] Membrane-electrode assemblies (MEAs) containing Pt/C as a cathode catalyst and Pt-free Pd/C as an anode catalyst were stacked between two current collectors containing graphite flow fields. The voltage of the fuel cell was changed between 0.4 and 1.0 V (*OCV*) or 0.4 and 1.4 V, and currents for each measurement were recorded on a potentiostat in real time. Each QXAFS oscillation at Pt L_{III}-edge measured for 15 s was divided into 15 fragments in *k* space and 15 fragments of QXAFS oscillations obtained by 15 different measurements were combined together into one interval. A series of TG-QXAFS with 1-s time resolution of a Pt/C cathode catalyst for a voltage-operating process from 0.4 to 1.0 V is presented in Figure 13b.

Time-resolved analyses of a Pt/C cathode fuel-cell catalyst yielded four parameters: (I) electrochemical charges in the fuel

cell recorded on the potentiostat, (II) the CNs and lengths of Pt–Pt bonds in the Pt nanoparticles, which reflect the particle size and stability of the Pt catalysts (EXAFS), (III) those of Pt–O bonds, which provide details of the reactions between H_2O as well as O_2 and the Pt-particle surface (EXAFS), and (IV) the electron density of Pt d orbitals (XANES). We have succeeded in determining the eight rate constants for the oxidation and reduction, which are related to the electron transfer, structural change, and d-electron density change at the Pt/C cathode catalyst, which are significantly different from each other. A hysteresis loop was found for the structural changes in the Pt cathode particles in the oxidation and reduction.

It should be noted that significant time lag between the four processes on the Pt/C cathode surface was observed. In the turning-off from 0.4 to 1.0 V (anode: H_2 and cathode: N_2), the reaction rates of electron transfer (k_{e1} and k_{e2}) were observed as 0.39 and 0.049 s^{-1}, respectively. After the fast electron transfer, the Pt particles were only slightly charged, and there were no chemical bonds with oxygen on the Pt surface at this stage. Pt–O bonds then slowly formed with the reaction rate $k_{(\text{Pt–O bond formation})}$ of 0.013 s^{-1} in conjunction with Pt charging with the reaction rate k_d of 0.011 s^{-1}, which was monitored by the d-electron density of states. The CN of the Pt–Pt bonds remained constant at about 9 between 0.4–1.0 V, which indicated that decomposition of the Pt catalyst or significant leaching to the electrolyte did not occur.[225]

When the cell voltage was increased to 1.4 V higher than the *OCV*, the Pt particles were gradually oxidized. The voltage operation from 0.4 to 1.4 V caused a decrease in the CN of the Pt–Pt bonds and an increase in the CN of the Pt–O bonds, and there changes slowly occurred at similar reaction rates as shown in Figure 13c ($k_{(\text{Pt–Pt bond dissociation})} = 0.031\ s^{-1}$ and $k_{(\text{Pt–O bond formation})} = 0.026\ s^{-1}$). The 20% decrease in the CN of the Pt–Pt bonds and the CN of 0.8 for the Pt–O bonds suggest that oxygen entered the subsurface of the Pt particles at 1.4 V.

Repeated voltage manipulations did not cause any decrease in electric charges, and the CN of Pt–Pt bonds recovered to its original value when the cell voltage returned to 0.4 V. The oxygen that entered the subsurface of the Pt nanoparticles was released, and the Pt particles kept their cubo-octahedron structures. The Pt ions did not dissolve into the electrolyte under N_2 atmosphere, although the voltage 1.4 V exceeded the threshold voltage for HO–H bond dissociation and promoted penetration of oxygen into the Pt subsurface.

In air, the bond behaviors at the cathode surface were distinct from those under N_2. When the cell voltage was increased to 1.4 V, the Pt–Pt bonds immediately broke and the CN of the Pt–Pt bonds did not recover even if the cell voltage was returned to 0.4 V. If a local inclination of electric potential forms on electrode surfaces, dissolution of the Pt catalysts gradually occurs, resulting in serious deterioration of Pt cathode catalysts. The in situ time-resolved TG-QXAFS under the fuel-cell operating conditions revealed the reaction kinetics of the fuel-cell Pt/C catalyst toward further development of practical fuel-cell catalysts.[225]

Summary

Surface-mediated design of catalytically active metal complexes and their structural kinetics under catalyst working conditions are reviewed. Metal-complex attachment and subsequent selective structural transformations often provide unique and regulated metal structures with remarkable catalytic activity. In situ characterization under catalyst working conditions revealed structural kinetics of these active metal species during catalysis and novel phenomena at catalyst surfaces. The strategies for surface-mediated selective catalysis, reaction-induced catalyst activation, photoinduced catalyst activation, surface functionalization using achiral molecules, chiral self-dimerization, molecular imprinting of supported metal complexes, and chemical vapor deposition of metal-cluster compounds would be promising to create novel metal catalysis for sustainable society.

The author thanks Prof. Yasuhiro Iwasawa, who is an emeritus professor of The University of Tokyo for his support. Prof. Takehiko Sasaki and Dr. Toshiaki Taniike at The University of Tokyo were consulted for DFT calculations. Prof. M. Nomura and Prof. Y. Inada at KEK-PF and Prof. M. Takata, Dr. T. Uruga, Dr. H. Tanida, and Dr. K. Kato at SPring-8 were consulted for time-resolved XAFS measurements. These works were supported by Grant-in-Aid for Scientific Research on Priority Areas (Concerto Catalysis) (No. 18065003) and (Coordination Space) (No. 18033011), Grant-in-Aid for Young Scientists (A) (No. 20686055), Grant-in-Aid for Scientific Research (S) (No. 18106013) from MEXT, Inoue Science Research Award from Inoue Foundation for Science, and JCII Subsidy System for Advanced Innovation in Chemical Industry. XAFS measurements were performed by the approval of PF-PAC (Nos. 2004G080, 2004G081, 2004G082, 2005G207, 2005G208, 2005G209, 2007G102, 2008G154, 2008G188, 2009G076, and 2009G080) and SPring-8 (Nos. 2005A0451, 2005A0452, 2007B1081, and 2009A1052).

References

1 Y. Iwasawa, *Tailored Metal Catalysts*, D. Reidel, Dordrecht, **1986**.
2 F. R. Hartley, *Supported Metal Complexes*, D. Reidel, Dordrecht, **1985**.
3 Y. Iwasawa, *Acc. Chem. Res.* **1997**, *30*, 103.
4 A. Corma, H. Garcia, *Adv. Synth. Catal.* **2006**, *348*, 1391.
5 J. M. Thomas, R. Raja, D. W. Lewis, *Angew. Chem., Int. Ed.* **2005**, *44*, 6456.
6 J. M. Notestein, A. Katz, *Chem.—Eur. J.* **2006**, *12*, 3954.
7 P. McMorn, G. J. Hutchings, *Chem. Soc. Rev.* **2004**, *33*, 108.
8 R. A. Sheldon, M. Wallau, I. W. C. E. Arends, U. Schuchardt, *Acc. Chem. Res.* **1998**, *31*, 485.
9 C. Copéret, J.-M. Basset, *Adv. Synth. Catal.* **2007**, *349*, 78.
10 J. C. Fierro-Gonzalez, S. Kuba, Y. Hao, B. C. Gates, *J. Phys. Chem. B* **2006**, *110*, 13326.
11 M. Tada, Y. Iwasawa, *Chem. Commun.* **2006**, 2833.
12 M. Ramin, J.-D. Grunwaldt, A. Baiker, *J. Catal.* **2005**, *234*, 256.
13 K. Yamaguchi, C. Yoshida, S. Uchida, N. Mizuno, *J. Am. Chem. Soc.* **2005**, *127*, 530.
14 C. Bianchini, V. Dal Santo, A. Meli, S. Moneti, M. Moreno, W. Oberhauser, R. Psaro, L. Sordelli, F. Vizza, *J. Catal.*

2003, *213*, 47.
15 F. Blanc, J. Thivolle-Cazat, J.-M. Basset, C. Copéret, A. S. Hock, Z. J. Tonzetich, R. R. Schrock, *J. Am. Chem. Soc.* **2007**, *129*, 1044.
16 A. Dorcier, N. Merle, M. Taoufik, F. Bayard, C. Lucas, A. de Mallmann, J. M. Basset, *Organometallics* **2009**, *28*, 2173.
17 B. M. L. Dioos, I. F. J. Vankelecom, P. A. Jacobs, *Adv. Synth. Catal.* **2006**, *348*, 1413.
18 S. Kobayashi, R. Akiyama, *Chem. Commun.* **2003**, 449.
19 S. Itsuno, *J. Synth. Org. Chem., Jpn.* **2009**, *67*, 1025.
20 T. Osako, Y. Uozumi, *Chem. Lett.* **2009**, *38*, 902.
21 M. R. Buchmeiser, *Chem. Rev.* **2009**, *109*, 303.
22 S. Tanaka, M. Tada, Y. Iwasawa, *J. Catal.* **2007**, *245*, 173.
23 M. Tada, R. Coquet, J. Yoshida, M. Kinoshita, Y. Iwasawa, *Angew. Chem., Int. Ed.* **2007**, *46*, 7220.
24 T. Hirakawa, S. Tanaka, N. Usuki, H. Kanzaki, M. Kishimoto, M. Kitamura, *Eur. J. Org. Chem.* **2009**, 789.
25 P. Barbaro, C. Bianchini, V. Dal Santo, A. Meli, S. Moneti, R. Psaro, A. Scaffidi, L. Sordelli, F. Vizza, *J. Am. Chem. Soc.* **2006**, *128*, 7065.
26 K. Kaneda, K. Mori, T. Mizugaki, K. Ebitani, *Curr. Org. Chem.* **2006**, *10*, 241.
27 J. M. Thomas, W. J. Thomas, *Principles and Practice of Heterogeneous Catalysis*, VCH Weinheim, **1997**.
28 M. Tada, Y. Iwasawa, *Annu. Rev. Mater. Res.* **2005**, *35*, 397.
29 M. Tada, Y. Iwasawa, *Coord. Chem. Rev.* **2007**, *251*, 2702.
30 M. Tada, M. Shimamoto, T. Sasaki, Y. Iwasawa, *Chem. Commun.* **2004**, 2562.
31 K. Asakura, K. Kitamura-Bando, Y. Iwasawa, H. Arakawa, K. Isobe, *J. Am. Chem. Soc.* **1990**, *112*, 9096.
32 J. Joubert, F. Delbecq, P. Sautet, E. Le Roux, M. Taoufik, C. Thieuleux, F. Blanc, C. Copéret, J. Thivolle-Cazat, J.-M. Basset, *J. Am. Chem. Soc.* **2006**, *128*, 9157.
33 C. A. Kruithof, M. A. Casado, G. Guillena, M. R. Egmond, A. van der Kerf-van Hoof, A. J. R. Heck, R. J. M. K. Gebbink, G. van Koten, *Chem.—Eur. J.* **2005**, *11*, 6869.
34 K.-J. Haack, S. Hashiguchi, A. Fujii, T. Ikariya, R. Noyori, *Angew. Chem., Int. Ed. Engl.* **1997**, *36*, 285.
35 M. Ito, S. Kitahara, T. Ikariya, *J. Am. Chem. Soc.* **2005**, *127*, 6172.
36 M. Ito, A. Sakaguchi, C. Kobayashi, T. Ikariya, *J. Am. Chem. Soc.* **2007**, *129*, 290.
37 M. Ito, A. Osaku, A. Shiibashi, T. Ikariya, *Org. Lett.* **2007**, *9*, 3711.
38 T. Ikariya, A. J. Blacker, *Acc. Chem. Res.* **2007**, *40*, 1300.
39 M. Ito, Y. Endo, T. Ikariya, *Organometallics* **2008**, *27*, 6053.
40 M. Tada, S. Muratsugu, M. Kinoshita, T. Sasaki, Y. Iwasawa, *J. Am. Chem. Soc.* **2010**, *132*, 713.
41 M. Tada, Y. Akatsuka, Y. Yang, T. Sasaki, M. Kinoshita, K. Motokura, Y. Iwasawa, *Angew. Chem., Int. Ed.* **2008**, *47*, 9252.
42 K. S. Kim, N. Winograd, *J. Catal.* **1974**, *35*, 66.
43 P. G. Gassman, C. H. Winter, *J. Am. Chem. Soc.* **1988**, *110*, 6130.
44 R. E. Shepherd, A. Proctor, W. W. Henderson, T. K. Myser, *Inorg. Chem.* **1987**, *26*, 2440.
45 L. Pu, *Chem. Rev.* **1998**, *98*, 2405.
46 Y. Chen, S. Yekta, A. K. Yudin, *Chem. Rev.* **2003**, *103*, 3155.
47 R. Noyori, *Asymmetric Catalysis in the Organic Synthesis*, Wiley, **1994**.
48 *Comprehensive Asymmetric Catalysis*, ed. by E. N. Jacobsen, A. Pfaltz, H. Yamamoto, Springer, **1999**.
49 D. A. Evans, W. C. Black, *J. Am. Chem. Soc.* **1993**, *115*, 4497.
50 Y. Morimoto, M. Iwahashi, K. Nishida, Y. Hayashi, H. Shirahama, *Angew. Chem., Int. Ed. Engl.* **1996**, *35*, 904.
51 D. A. Evans, S. J. Miller, T. Lectka, P. von Matt, *J. Am. Chem. Soc.* **1999**, *121*, 7559.
52 D. A. Evans, D. M. Barnes, J. S. Johnson, T. Lectka, P. von Matt, S. J. Miller, J. A. Murry, R. D. Norcross, E. A. Shaughnessy, K. R. Campos, *J. Am. Chem. Soc.* **1999**, *121*, 7582.
53 D. A. Evans, J. S. Johnson, E. J. Olhava, *J. Am. Chem. Soc.* **2000**, *122*, 1635.
54 J. M. Takacs, E. C. Lawson, M. J. Reno, M. A. Youngman, D. A. Quincy, *Tetrahedron: Asymmetry* **1997**, *8*, 3073.
55 A. K. Ghosh, H. Cho, J. Cappiello, *Tetrahedron: Asymmetry* **1998**, *9*, 3687.
56 J. Zhou, Y. Tang, *Org. Biomol. Chem.* **2004**, *2*, 429.
57 A. K. Ghosh, P. Mathivanan, J. Cappiello, *Tetrahedron: Asymmetry* **1998**, *9*, 1.
58 K. C. Nicolaou, S. A. Snyder, T. Montagnon, G. Vassilikogiannakis, *Angew. Chem., Int. Ed.* **2002**, *41*, 1668.
59 K. Takao, R. Munakata, K. Tadano, *Chem. Rev.* **2005**, *105*, 4779.
60 J. M. Fraile, J. I. García, M. A. Harmer, C. I. Herrerías, J. A. Mayoral, *J. Mol. Catal. A: Chem.* **2001**, *165*, 211.
61 P. O'Leary, N. P. Krosveld, K. P. de Jong, G. van Koten, R. J. M. Klein Gebbink, *Tetrahedron Lett.* **2004**, *45*, 3177.
62 A. Corma, H. García, A. Moussaif, M. J. Sabater, R. Zniber, A. Redouane, *Chem. Commun.* **2002**, 1058.
63 Y. Traa, D. M. Murphy, R. D. Farley, G. J. Hutchings, *Phys. Chem. Chem. Phys.* **2001**, *3*, 1073.
64 S. Taylor, J. Gullick, P. McMorn, D. Bethell, P. C. Bulman Page, F. E. Hancock, F. King, G. J. Hutchings, *J. Chem. Soc., Perkin Trans. 2* **2001**, 1724.
65 Y. Wan, P. McMorn, F. E. Hancock, G. J. Hutchings, *Catal. Lett.* **2003**, *91*, 145.
66 R. Annunziata, M. Benaglia, M. Cinquini, F. Cozzi, M. Pitillo, *J. Org. Chem.* **2001**, *66*, 3160.
67 K. Hallman, C. Moberg, *Tetrahedron: Asymmetry* **2001**, *12*, 1475.
68 M. Tada, S. Tanaka, Y. Iwasawa, *Chem. Lett.* **2005**, *34*, 1362.
69 M. Soibinet, I. Déchamps-Olivier, A. Nohamadou, M. Aplincourt, *Inorg. Chem. Commun.* **2004**, *7*, 405.
70 M. D. Jones, R. Raja, J. M. Thomas, B. F. G. Johnson, D. W. Lewis, J. Rouzaud, K. D. M. Harris, *Angew. Chem., Int. Ed.* **2003**, *42*, 4326.
71 J. M. Thomas, R. Raja, D. W. Lewis, *Angew. Chem., Int. Ed.* **2005**, *44*, 2562.
72 M. Tada, T. Taniike, L. M. Kantam, Y. Iwasawa, *Chem. Commun.* **2004**, 2542.
73 M. Tada, N. Kojima, Y. Izumi, T. Taniike, Y. Iwasawa, *J. Phys. Chem. B* **2005**, *109*, 9905.
74 J. Bao, W. D. Wulff, A. L. Rheingold, *J. Am. Chem. Soc.* **1993**, *115*, 3814.
75 R. Noyori, H. Takaya, *Acc. Chem. Res.* **1990**, *23*, 345.
76 H.-U. Blaser, *Chem. Rev.* **1992**, *92*, 935.
77 G. Kaupp, *Angew. Chem., Int. Ed. Engl.* **1994**, *33*, 728.
78 R. Pummerer, E. Prell, A. Rieche, *Ber. Dtsch. Chem. Ges.* **1926**, *59*, 2159.
79 M. J. S. Dewar, T. Nakaya, *J. Am. Chem. Soc.* **1968**, *90*, 7134.

80 B. Feringa, H. Wynberg, *Bioorg. Chem.* **1978**, *7*, 397.
81 E. Armengol, A. Corma, H. García, J. Primo, *Eur. J. Org. Chem.* **1999**, 1915.
82 K. Ding, Y. Wang, L. Zhang, Y. Wu, T. Matsuura, *Tetrahedron* **1996**, *52*, 1005.
83 K. Yamamoto, H. Fukushima, Y. Okamoto, K. Hatada, M. Nakazaki, *J. Chem. Soc., Chem. Commun.* **1984**, 1111.
84 M. Nakajima, I. Miyoshi, K. Kanayama, S. Hashimoto, M. Noji, K. Koga, *J. Org. Chem.* **1999**, *64*, 2264.
85 X. Lin, J. Yang, M. C. Kozlowski, *Org. Lett.* **2001**, *3*, 1137.
86 R. Irie, K. Masutani, T. Katsuki, *Synlett* **2000**, 1433.
87 C.-Y. Chu, D.-R. Hwang, S.-K. Wnag, B.-J. Uang, *Chem. Commun.* **2001**, 980.
88 S.-W. Hon, C.-H. Li, J.-H. Kuo, N. B. Barhate, Y.-H. Liu, Y. Wang, C.-T. Chen, *Org. Lett.* **2001**, *3*, 869.
89 Z. Luo, Q. Liu, L. Gong, X. Cui, A. Mi, Y. Jiang, *Angew. Chem., Int. Ed.* **2002**, *41*, 4532.
90 S. Murakami, S. Habaue, H. Higashimura, *Polymer* **2007**, *48*, 6565.
91 S. Takizawa, T. Katayama, H. Somei, Y. Asano, T. Yoshida, C. Kameyama, D. Rajesh, K. Onitsuka, T. Suzuki, M. Mikami, H. Yamataka, D. Jayaprakash, H. Sasai, *Tetrahedron* **2008**, *64*, 3361.
92 S. Takizawa, T. Katayama, C. Kameyama, K. Onitsuka, T. Suzuki, T. Yanagida, T. Kawai, H. Sasai, *Chem. Commun.* **2008**, 1810.
93 S. Takizawa, T. Katayama, H. Sasai, *Chem. Commun.* **2008**, 4113.
94 S. Takizawa, D. Rajesh, T. Katayama, H. Sasai, *Synlett* **2009**, 1667.
95 S. S. Eaton, K. M. More, B. M. Sawant, G. R. Eaton, *J. Am. Chem. Soc.* **1983**, *105*, 6560.
96 A. Katz, M. E. Davis, *Nature* **2000**, *403*, 286.
97 P. A. Brady, J. K. M. Sanders, *Chem. Soc. Rev.* **1997**, *26*, 327.
98 D. C. Sherrington, *Chem. Commun.* **1998**, 2275.
99 M. E. Davis, A. Katz, W. R. Ahmad, *Chem. Mater.* **1996**, *8*, 1820.
100 B. Sellergren, *Angew. Chem., Int. Ed.* **2000**, *39*, 1031.
101 M. J. Whitcombe, C. Alexander, E. N. Vulfson, *Synlett* **2000**, 911.
102 K. Haupt, K. Mosbach, *Chem. Rev.* **2000**, *100*, 2495.
103 J. D. Marty, M. Mauzac, *Adv. Polym. Sci.* **2005**, *172*, 1.
104 J. J. Becker, M. R. Gagne, *Acc. Chem. Res.* **2004**, *37*, 798.
105 C. Alexander, L. Davidson, W. Hayes, *Tetrahedron* **2003**, *59*, 2025.
106 C. Alexander, H. S. Andersson, L. I. Andersson, R. J. Ansell, N. Kirsch, I. A. Nicholls, J. O'Mahony, M. J. Whitcombe, *J. Mol. Recognit.* **2006**, *19*, 106.
107 X. J. Wang, Z. L. Xu, Z. G. Yang, N. C. Bing, *Prog. Chem.* **2007**, *19*, 805.
108 L. Ye, K. Mosbach, *Chem. Mater.* **2008**, *20*, 859.
109 R. Gupta, A. Kumar, *Biotechnol. Adv.* **2008**, *26*, 533.
110 A. Walcarius, M. M. Collinson, *Annu. Rev. Anal. Chem.* **2009**, *2*, 121.
111 M. Komiyama, T. Takeuchi, T. Mukawa, H. Asanuma, *Molecular Imprinting*, Wiley-VCH, **2003**.
112 Y. Ge, A. P. F. Turner, *Chem.—Eur. J.* **2009**, *15*, 8100.
113 K. Morihara, M. Kurosawa, Y. Kamata, T. Shimada, *J. Chem. Soc., Chem. Commun.* **1992**, 358.
114 J. Heilmann, W. F. Maier, *Angew. Chem., Int. Ed. Engl.* **1994**, *33*, 471.
115 A. G. Strikovsky, D. Kasper, M. Grün, B. S. Green, J. Hradil, G. Wulff, *J. Am. Chem. Soc.* **2000**, *122*, 6295.
116 M. A. Markowitz, P. R. Kust, G. Deng, P. E. Schoen, J. S. Dordick, D. S. Clark, B. P. Gaber, *Langmuir* **2000**, *16*, 1759.
117 T. Tanimura, N. Katada, M. Niwa, *Langmuir* **2000**, *16*, 3858.
118 J. Matsui, I. A. Nicholls, I. Karube, K. Mosbach, *J. Org. Chem.* **1996**, *61*, 5414.
119 F. Locatelli, P. Gamez, M. Lemaire, *J. Mol. Catal. A: Chem.* **1998**, *135*, 89.
120 B. P. Santora, A. O. Larsen, M. R. Gagné, *Organometallics* **1998**, *17*, 3138.
121 K. Polborn, K. Severin, *Chem.—Eur. J.* **2000**, *6*, 4604.
122 A. N. Cammidge, N. J. Baines, R. K. Bellingham, *Chem. Commun.* **2001**, 2588.
123 Z. Meng, T. Yamazaki, K. Sode, *Biotechnol. Lett.* **2003**, *25*, 1075.
124 E. Burri, M. Ohm, C. Daguenet, K. Severin, *Chem.—Eur. J.* **2005**, *11*, 5055.
125 J. Lee, S. Bernard, X.-C. Liu, *React. Funct. Polym.* **2009**, *69*, 650.
126 M. Tada, Y. Iwasawa, *J. Mol. Catal. A: Chem.* **2003**, *199*, 115.
127 M. Tada, T. Sasaki, T. Shido, Y. Iwasawa, *Phys. Chem. Chem. Phys.* **2002**, *4*, 5899.
128 M. Tada, T. Sasaki, Y. Iwasawa, *J. Catal.* **2002**, *211*, 496.
129 M. Tada, T. Sasaki, Y. Iwasawa, *Phys. Chem. Chem. Phys.* **2002**, *4*, 4561.
130 M. Tada, T. Sasaki, Y. Iwasawa, *J. Phys. Chem. B* **2004**, *108*, 2918.
131 *Multimetallic Catalysts in Organic Synthesis*, ed. by M. Shibasaki, Y. Yamamoto, Wiley-VCH, **2004**.
132 M. Tada, Y. Iwasawa, *Supported Catalysts from Chemical Vapor Deposition and Related Techniques*, in *Handbook of Heterogeneous Catalysis*, 2nd ed., ed. by G. Ertl, H. Knozinger, F. Schuth, J. Weitkamp, Wiley-VCH, **2007**, p. 539.
133 M. Tada, T. Taniike, Y. Iwasawa, *J. Phys. Chem. C* **2007**, *111*, 11663.
134 R. Bal, M. Tada, T. Sasaki, Y. Iwasawa, *Angew. Chem., Int. Ed.* **2006**, *45*, 448.
135 M. Tada, R. Bal, Y. Iwasawa, *Catal. Today* **2006**, *117*, 141.
136 M. Tada, R. Bal, T. Sasaki, Y. Uemura, Y. Inada, S. Tanaka, M. Nomura, Y. Iwasawa, *J. Phys. Chem. C* **2007**, *111*, 10095.
137 Y. Iwasawa, in *Elementary Reaction Steps in Heterogeneous Catalysis*, ed. by R. W. Joyner, R. A. van Santen, NATO ASI Series C, NATO, **1993**, Vol. 398, p. 287.
138 Y. Iwasawa, *Stud. Surf. Sci. Catal.* **1996**, *101*, 21.
139 Y. Iwasawa, *Adv. Catal.* **1987**, *35*, 187.
140 J. M. Thomas, R. Raja, G. Sankar, R. G. Bell, *Nature* **1999**, *398*, 227.
141 R. Raja, G. Sankar, J. M. Thomas, *Angew. Chem., Int. Ed.* **2000**, *39*, 2313.
142 A. Yamaguchi, K. Asakura, Y. Iwasawa, *J. Mol. Catal. A: Chem.* **1999**, *146*, 65.
143 A. Yamaguchi, T. Shido, K. Asakura, Y. Iwasawa, *Stud. Surf. Sci. Catal.* **2000**, *130*, 605.
144 T. Shido, A. Yamaguchi, K. Asakura, Y. Iwasawa, *J. Mol. Catal. A: Chem.* **2000**, *163*, 67.
145 Y. Iwasawa, M. Yamada, Y. Sato, H. Kuroda, *J. Mol. Catal.* **1984**, *23*, 95.
146 T. Taniike, M. Tada, Y. Morikawa, T. Sasaki, Y. Iwasawa, *J. Phys. Chem. B* **2006**, *110*, 4929.
147 T. Taniike, M. Tada, R. Coquet, Y. Morikawa, T. Sasaki, Y.

Iwasawa, *Chem. Phys. Lett.* **2007**, *443*, 66.
148 Y.-J. Seo, Y. Mukai, T. Tagawa, S. Goto, *J. Mol. Catal. A: Chem.* **1997**, *120*, 149.
149 T. Miyahara, H. Kanzaki, R. Hamada, S. Kuroiwa, S. Nishiyama, S. Tsuruya, *J. Mol. Catal. A: Chem.* **2001**, *176*, 141.
150 H. Yamanaka, R. Hamada, H. Nibuta, S. Nishiyama, S. Tsuruya, *J. Mol. Catal. A: Chem.* **2002**, *178*, 89.
151 T. Kusakari, T. Sasaki, Y. Iwasawa, *Chem. Commun.* **2004**, 992.
152 S. Sumimoto, C. Tanaka, S. Yamaguchi, Y. Ichihashi, S. Nishiyama, S. Tsuruya, *Ind. Eng. Chem. Res.* **2006**, *45*, 7444.
153 Y. Liu, K. Murata, M. Inaba, *J. Mol. Catal. A: Chem.* **2006**, *256*, 247.
154 Y.-J. Seo, T. Tagawa, S. Goto, *J. Chem. Eng. Jpn.* **1994**, *27*, 307.
155 D. H. Bremner, A. E. Burgess, F.-B. Li, *Appl. Catal., A* **2000**, *203*, 111.
156 S. Jiang, Y. Kong, C. Wu, Z. Xu, H. Y. Zhu, C. Y. Wang, J. Wang, Q. J. Yan, *Chin. J. Catal.* **2006**, *27*, 421.
157 T. Mizuno, H. Yamada, T. Tagawa, S. Goto, *J. Chem. Eng. Jpn.* **2005**, *38*, 849.
158 M. Jian, L. Zhu, J. Wang, J. Zhang, G. Li, C. Hu, *J. Mol. Catal. A: Chem.* **2006**, *253*, 1.
159 K. Sato, T. Hanaoka, S. Hamakawa, M. Nishioka, K. Kobayashi, T. Inoue, T. Namba, F. Mizukami, *Catal. Today* **2006**, *118*, 57.
160 X. Gao, J. Xu, *Appl. Clay Sci.* **2006**, *33*, 1.
161 R. Molinari, T. Poerio, P. Argurio, *Catal. Today* **2006**, *118*, 52.
162 N. I. Rudakova, M. V. Klyuev, Y. G. Erykalov, D. N. Ramazanov, *Russ. J. Gen. Chem.* **2006**, *76*, 1407.
163 G. I. Panov, G. A. Sheveleva, A. S. Kharitonov, V. N. Romannikov, L. A. Vostrikova, *Appl. Catal., A* **1992**, *82*, 31.
164 G. I. Panov, *CATTECH* **2000**, *4*, 18.
165 J. L. Motz, H. Heinichen, W. F. Hölderich, *J. Mol. Catal. A: Chem.* **1998**, *136*, 175.
166 W. F. Hölderich, *Catal. Today* **2000**, *62*, 115.
167 G. Centi, C. Genovese, G. Giordano, A. Katovic, S. Perathoner, *Catal. Today* **2004**, *91–92*, 17.
168 E. J. M. Hensen, Q. Zhu, R. A. van Santen, *J. Catal.* **2005**, *233*, 136.
169 F. Kollmer, H. Hausmann, W. F. Hölderich, *J. Catal.* **2004**, *227*, 398.
170 E. J. M. Hensen, Q. Zhu, R. A. van Santen, *J. Catal.* **2003**, *220*, 260.
171 G. Centi, S. Perathoner, R. Arrigo, G. Giordano, A. Katovic, V. Pedulà, *Appl. Catal., A* **2006**, *307*, 30.
172 N. R. Shiju, S. Fiddy, O. Sonntag, M. Stockenhuber, G. Sanker, *Chem. Commun.* **2006**, 4955.
173 S. Niwa, M. Eswaramoorthy, J. Nair, A. Raj, N. Itoh, H. Shoji, T. Namba, F. Mizukami, *Science* **2002**, *295*, 105.
174 H. Ehrich, H. Berndt, M.-M. Pohl, K. Jähnisch, M. Baerns, *Appl. Catal., A* **2002**, *230*, 271.
175 M. Tani, T. Sakamoto, S. Mita, S. Sakaguchi, Y. Ishii, *Angew. Chem., Int. Ed.* **2005**, *44*, 2586.
176 T. Dong, J. Li, F. Huang, L. Wang, J. Tu, Y. Torimoto, M. Sadakata, Q. Li, *Chem. Commun.* **2005**, 2724.
177 J. Haggin, *Chem. Eng. News* **1993**, 23.
178 B. Cornils, W. A. Herrmann, *J. Catal.* **2003**, *216*, 23.
179 B. Lücke, K. V. Narayana, A. Martin, K. Jähnisch, *Adv. Synth. Catal.* **2004**, *346*, 1407.
180 C. C. Romão, F. E. Kühn, W. A. Herrmann, *Chem. Rev.* **1997**, *97*, 3197.
181 J. Okal, J. Baran, *J. Catal.* **2001**, *203*, 466.
182 *Modern Oxidation Methods*, ed. by J.-E. Backvall, Wiley-VCH, **2004**.
183 *Modern Heterogeneous Oxidation Catalysis*, ed. by N. Mizuno, Wiley-VCH, **2009**.
184 D. Mandelli, M. C. A. van Vliet, U. Arnold, R. A. Sheldon, U. Schuchardt, *J. Mol. Catal. A: Chem.* **2001**, *168*, 165.
185 A. Salameh, C. Copéret, J.-M. Basset, V. P. W. Böhm, M. Röper, *Adv. Synth. Catal.* **2007**, *349*, 238.
186 H. C. Lo, H. Han, L. J. D'Souza, S. C. Sinha, E. Keinan, *J. Am. Chem. Soc.* **2007**, *129*, 1246.
187 M. Onaka, T. Oikawa, *Chem. Lett.* **2002**, 850.
188 Y. Yuan, T. Shido, Y. Iwasawa, *Chem. Commun.* **2000**, 1421.
189 Y. Yuan, Y. Iwasawa, *J. Phys. Chem. B* **2002**, *106*, 4441.
190 H. Liu, H. Imoto, T. Shido, Y. Iwasawa, *J. Catal.* **2001**, *200*, 69.
191 N. Viswanadham, T. Shido, Y. Iwasawa, *Appl. Catal., A* **2001**, *219*, 223.
192 N. Viswanadham, T. Shido, T. Sasaki, Y. Iwasawa, *J. Phys. Chem. B* **2002**, *106*, 10955.
193 T. Matsushita, R. P. Phizackerley, *Jpn. J. Appl. Phys.* **1981**, *20*, 2223.
194 U. Kaminaga, T. Matsushita, K. Kohra, *Jpn. J. Appl. Phys.* **1981**, *20*, L355.
195 Y. Iwasawa, *J. Catal.* **2003**, *216*, 165.
196 M. A. Newton, A. J. Dent, J. Evans, *Chem. Soc. Rev.* **2002**, *31*, 83.
197 Y. Iwasawa, A. Suzuki, M. Nomura, *Phys. Scr.* **2005**, 59.
198 J. Evans, A. Puig-Molina, M. Tromp, *MRS Bull.* **2007**, *32*, 1038.
199 A. Yamaguchi, T. Shido, Y. Inada, T. Kogure, K. Asakura, M. Nomura, Y. Iwasawa, *Catal. Lett.* **2000**, *68*, 139.
200 A. Yamaguchi, T. Shido, Y. Inada, T. Kogure, K. Asakura, M. Nomura, Y. Iwasawa, *Bull. Chem. Soc. Jpn.* **2001**, *74*, 801.
201 A. Yamaguchi, A. Suzuki, T. Shido, Y. Inada, K. Asakura, M. Nomura, Y. Iwasawa, *J. Phys. Chem. B* **2002**, *106*, 2415.
202 C. Lamberti, C. Prestipino, F. Bonino, L. Capello, S. Bordiga, G. Spoto, A. Zecchina, S. D. Moreno, B. Cremaschi, M. Garilli, A. Marsella, D. Carmello, S. Vidotto, G. Leofanti, *Angew. Chem., Int. Ed.* **2002**, *41*, 2341.
203 A. Suzuki, Y. Inada, A. Yamaguchi, T. Chihara, Y. Iwasawa, *Angew. Chem., Int. Ed.* **2003**, *42*, 4795.
204 M. A. Newton, B. Jyoti, A. J. Dent, S. G. Fiddy, J. Evans, *Chem. Commun.* **2004**, 2382.
205 A. Suzuki, Y. Yamaguchi, T. Chihara, Y. Inada, M. Yuasa, M. Abe, M. Nomura, Y. Iwasawa, *J. Phys. Chem. B* **2004**, *108*, 5609.
206 X. Wang, J. A. Rodriguez, J. C. Hanson, M. Pérez, J. Evans, *J. Chem. Phys.* **2005**, *123*, 221101.
207 O. Friedrichs, D. Martínez-Martínez, G. Guilera, J. C. S. López, A. Fernández, *J. Phys. Chem. C* **2007**, *111*, 10700.
208 T. Yamamoto, A. Suzuki, Y. Nagai, T. Tanabe, F. Dong, Y. Inada, M. Nomura, M. Tada, Y. Iwasawa, *Angew. Chem., Int. Ed.* **2007**, *46*, 9253.
209 K. Okumura, T. Honma, S. Hirayama, T. Sanada, M. Niwa, *J. Phys. Chem. C* **2008**, *112*, 16740.
210 K. Teramura, S. Okuoka, S. Yamazoe, K. Kato, T. Shishido, T. Tanaka, *J. Phys. Chem. C* **2008**, *112*, 8495.
211 M. Harada, Y. Inada, *Langmuir* **2009**, *25*, 6049.
212 A. Z. Weber, J. Newman, *Chem. Rev.* **2004**, *104*, 4679.

213 C.-Y. Wang, *Chem. Rev.* **2004**, *104*, 4727.
214 M. Z. Jacobson, W. G. Colella, D. M. Golden, *Science* **2005**, *308*, 1901.
215 B. C. H. Steele, A. Heinzel, *Nature* **2001**, *414*, 345.
216 *Electrocatalysis*, ed. by J. Lipkowski, P. N. Ross, Wiley-VCH, **1998**.
217 L. Zhang, S. Mukerjee, *J. Electrochem. Soc.* **2006**, *153*, A1062.
218 P. J. Ferreira, G. J. la O', Y. Shao-Horn, D. Morgan, R. Makharia, S. Kocha, H. Gasteiger, *J. Electrochem. Soc.* **2005**, *152*, A2256.
219 A. E. Russell, A. Rose, *Chem. Rev.* **2004**, *104*, 4613.
220 Y. Zhang, M. L. Toebes, A. van der Eerden, W. E. O'Grady, K. P. de Jong, D. C. Koningsberger, *J. Phys. Chem. B* **2004**, *108*, 18509.
221 H. Yoshitake, T. Mochizuki, O. Yamazaki, K. Ota, *J. Electroanal. Chem.* **1993**, *361*, 229.
222 C. Roth, N. Martz, T. Buhrmester, J. Scherer, H. Fuess, *Phys. Chem. Chem. Phys.* **2002**, *4*, 3555.
223 V. S. Murthi, R. C. Urian, S. Mukerjee, *J. Phys. Chem. B* **2004**, *108*, 11011.
224 W.-S. Yoon, J. Hanson, J. McBreen, X.-Q. Yang, *Electrochem. Commun.* **2006**, *8*, 859.
225 M. Tada, S. Murata, T. Asaoka, K. Hiroshima, K. Okumura, H. Tanida, T. Uruga, H. Nakanishi, S. Matsumoto, Y. Inada, M. Nomura, Y. Iwasawa, *Angew. Chem., Int. Ed.* **2007**, *46*, 4310.

Mizuki Tada was received her Ph.D. in 2005 from The University of Tokyo. Since 2004, she worked in Department of Chemistry, The University of Tokyo as assistant professor. Since 2008, she promoted to associate professor of chemistry at The University of Tokyo. She moved to Institute for Molecular Science as associate professor in 2008. She awarded Inoue Foundation Award for Young Scientists (2007), PCCP Prize from Royal Society of Chemistry (2007), CSJ Award for Young Chemists (2007), The Lectureship of The University of Tokyo (2008), Inoue Research Award (2009), and Young Scientist's Prize of The Commendation for Science and Technology by the Minister of Education, Culture, Sports, Science and Technology, Japan (2010).